

## TRANSPORT PROCESSES IN STARS: DIFFUSION, ROTATION, MAGNETIC FIELDS AND INTERNAL WAVES

Suzanne Talon<sup>1</sup>

**Abstract.** In this paper, I explore various transport processes that have a large impact of the distribution of elements inside stars and thus, on stellar evolution. A heuristic description of the physics behind equations is provided, and key references are given. Finally, for each process, I will briefly review (some) important results as well as discuss directions for future work.

### 1 Atomic diffusion

#### 1.1 Introduction

Atomic diffusion refers to atomic scale physical processes that cause the stratification of various species and the smoothing of chemical discontinuities. These processes occur when multicomponent plasmas are subject to physical conditions that vary within the medium (such as pressure, temperature or density) or are subject to external forces that vary from species to species and are related to the Brownian motions of particles. Stellar interiors are a good laboratory for the study of these processes.

As atomic diffusion is not the main subject of this paper, this section will briefly outline general ideas to keep in mind when diffusion<sup>1</sup> is mentioned. Calculations are presented for a small concentration of particles  $i$  diffusing in protons  $p$ . This is called the *trace element approximation*. For a more complete description of diffusion in a general context see Burgers (1969) or Chapman & Cowling (1970).

---

<sup>1</sup> Département de physique, Université de Montréal, C.P. 6128, succursale centre-ville, Montréal, Québec, H3C 3J8

<sup>1</sup>Let us note that atomic diffusion is generally referred to simply as *diffusion*.

### 1.2 Diffusion and external forces

We first consider a gas in which physical parameters are constant and some external force  $\mathcal{F}_{\text{ext}_i}$  is exerted on particles  $i$ . The total force on  $i$  is then

$$\mathcal{F}_i = -k_B T \frac{\partial \ln P_i}{\partial r} + \mathcal{F}_{\text{ext}_i} \quad (1.1)$$

where  $P_i$  represents the partial pressure on  $i$ , and is related to the total pressure  $P$  and the concentration  $c_i$  by

$$c_i = \frac{P_i}{P_p + P_i} \quad \text{with } P_i \ll P_p. \quad (1.2)$$

Equilibrium is obtained when  $\mathcal{F}_i = 0$ . Since diffusion is a slow process that should bring composition gradients to their equilibrium values, it is reasonable to assume that the diffusion velocity  $V_{ip}$  of  $i$  with respect to protons is proportional to the difference between actual and equilibrium values (Eddington 1930) and thus

$$V_{ip} = D_{\text{at}} \left[ -\frac{\partial \ln c_i}{\partial r} + \frac{\mathcal{F}_{\text{ext}_i}}{k_B T} \right] \quad (1.3)$$

and the change of  $c_i$  during this evolution is given by<sup>2</sup>

$$\frac{\partial c_i}{\partial t} = -\frac{\partial}{\partial r} (V_{ip} c_i). \quad (1.4)$$

The atomic diffusion coefficient is  $D_{\text{at}} = \frac{1}{3} \Lambda v_T$  with  $\Lambda$  the particle mean free path and  $v_T$  the thermal velocity (see *e.g.* Aller & Chapman 1960). In the absence of an external force, this equation shows the tendency of microscopic motions to eliminate abundance gradients.

### 1.3 Gravitational settling and radiative forces

Let us now look at two specific external forces encountered in stellar interiors. First, we have gravity. When the mean molecular mass of the stellar plasma  $\mu$  is different from the mass of  $i$  ( $m_i$ ), the differential force on  $i$  is

$$\mathcal{F}_{\text{ext}_i} = \mu g - m_i g = (\mu - m_i) g \quad (1.5)$$

where we used again the perfect gas law, and assumed hydrostatic equilibrium.  $g$  is the local gravitational acceleration. In stars, this equation implies that elements heavier than hydrogen must “fall” towards the star’s center, and this is called *gravitational settling*.

The other force that has a large impact on element stratification is the transfer of momentum caused by photon absorption. In the region where radiative transfer

---

<sup>2</sup>Here, modifications of the structure are neglected.

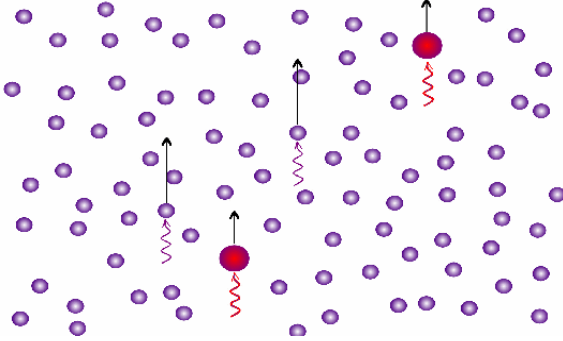


**Fig. 1.** The absorption of photons of different energies by various atomic species causes an acceleration that opposes gravity. When absorption is more probable, and the number of absorbers is small, this may produce their *radiative levitation*.

can be described using the diffusion approximation, the star's thermal structure is calculated using the *Rosseland mean opacity*  $\kappa_R$  defined as

$$\frac{1}{\kappa_R} \int_0^\infty \frac{\partial B(\nu, T)}{\partial T} d\nu = \int_0^\infty \frac{1}{\kappa_\nu} \frac{\partial B(\nu, T)}{\partial T} d\nu \quad (1.6)$$

where  $B(\nu, T)$  is the Planck function and  $\kappa_\nu$  the monochromatic opacity. The radiative luminosity  $L^{\text{rad}}$  is then related to the temperature gradient by

$$L^{\text{rad}} = -\frac{64\pi\sigma_R r^2}{3} \frac{T^3}{\kappa_R \rho} \frac{dT}{dr} \quad (1.7)$$

where  $\sigma_R$  is the Stefan-Boltzmann constant. For a given element  $i$ , the absorbed momentum is proportional to the fraction  $f_i$  of the total flux that is absorbed<sup>3</sup> by that type of particle. We can now compute the radiative acceleration of particle  $i$  as

$$g_{\text{rad}i} = \frac{1}{4\pi r^2} \frac{L^{\text{rad}}}{c} \kappa_R \frac{f_i}{X_i} \quad (1.8)$$

where

$$f_i = \int_0^\infty \frac{\kappa_{\nu i}}{\kappa_\nu} \mathcal{P}(u) du \quad \text{with} \quad \int_0^\infty \mathcal{P}(u) du = 1 \quad (1.9)$$

where  $u = h\nu/k_B T$  and  $\mathcal{P}(u) = \frac{15}{4\pi^4} \frac{u^4 e^u}{(e^u - 1)^2}$  is the normalized radiation flux associated with the temperature derivative of the Planck function (this was derived first by Michaud et al. 1976). The calculation of radiative forces thus requires detailed spectra for all species and all ionization states.

<sup>3</sup>This is in fact an approximation. The complete treatment involves momentum redistribution between ions and electrons (see Richer et al. 1998 for details).

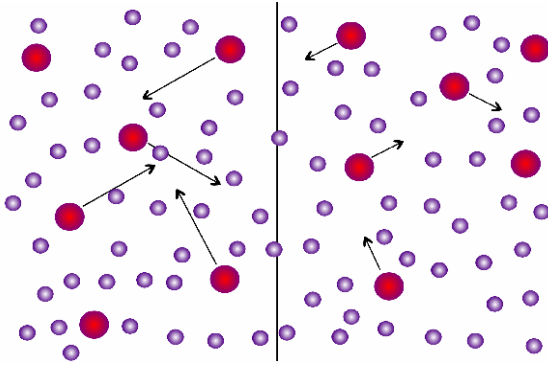


**Fig. 2.** When temperature is not homogeneous, the particles mean free path varies. In this cartoon, the probability of crossing the line to the left is different from the probability of crossing it to the right if the abundance is homogeneous. The achievement of equilibrium requires that there be a lower density of big particles on the left than on the right.

For a given trace element, when  $g_{\text{rad}} > g$ , the element will be “supported” by radiation, and will move upwards toward regions of force neutrality ( $g_{\text{rad}} \simeq g$ ); this neutrality condition may also result from absorption saturation<sup>4</sup>. In the opposite case ( $g_{\text{rad}} < g$ ), elements sink.

#### 1.4 Diffusion and temperature gradients

Temperature gradients are another source of element stratification. In a binary fluid (with all other physical parameters constant), the particles mean free path depend on temperature through their collision cross section (roughly as  $\sigma \propto T^{-2}$  for ions, while it does not depend on  $T$  for neutral atoms) and through their thermal velocity ( $v_T \propto T^{1/2}$ ).

The efficiency of this process can be estimated by considering the net flux of ions through an equipotential (Vauclair, 1983)

$$n_i V_i = \frac{1}{6} v_T|_{r+\Lambda} n_i|_{r+\Lambda} \frac{\sigma|_{r+\Lambda}}{\sigma|_r} - \frac{1}{6} v_T|_{r-\Lambda} n_i|_{r-\Lambda} \frac{\sigma|_{r-\Lambda}}{\sigma|_r} \quad (1.10)$$

where  $n_i$  is the number density and assuming that on average 1/6 of ions move in the direction of the equipotential. If  $n_i$  is fixed, this is simply

$$V_i = \frac{\Lambda}{3\sigma} \frac{\partial(v_T\sigma)}{\partial r} \simeq -\frac{1}{2} D_{\text{at}} \frac{\partial \ln T}{\partial r} \quad (1.11)$$

<sup>4</sup>As atoms migrate upwards and  $X_i$  rises, they have to share the momentum that photons give away, potentially leading to a saturation of  $g_{\text{rad}}$  which limits further growth of  $X_i$ .

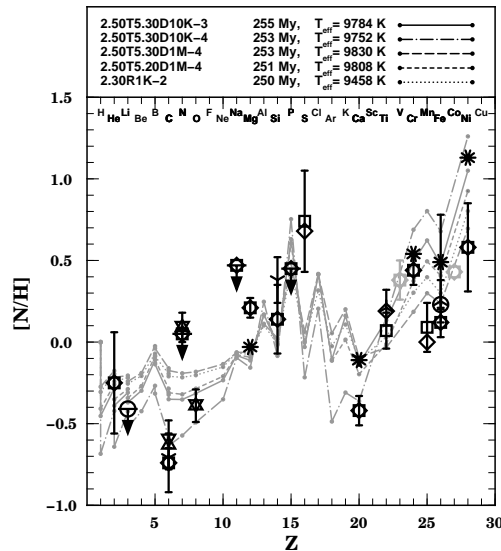


**Fig. 3.** Surface abundances in Sirius under the effect of atomic diffusion including radiative forces and some ad-hoc turbulence (various lines) compared with observations by various authors (symbols). (Figure 18 of Richer et al. 2000.)

for ions. A realistic calculation would give a leading factor of  $2.65(Z_i/Z_p)^2$  instead of the 2 given here. In more general conditions, even the sign in Eq. (1.11) may be different as it depends on the masses of the colliding particles. This is discussed at length for example in Michaud (1993).

### 1.5 Some applications of diffusion theory

Diffusion theory has been applied to a wide variety of stars. Its effects are expected to be largest in stars which have only shallow surface convection zones. This is the case in particular of AmFm stars, which exhibit abundance anomalies that can be as large as one order of magnitude for certain elements and thus, it is believed that these are only superficial. The Montreal group calculated stellar models including all effects of atomic diffusion, including radiative accelerations (Richer, Michaud & Turcotte, 2000). One of their results is shown on Fig. 3. When radiative forces alone are considered, the predicted anomalies are too large by a factor of  $\sim 3$ . In the results shown here, a small amount of ad-hoc turbulence has been added to obtain a good agreement with the observations.

Diffusion theory has also been applied to solar models. There, it predicts the settling of helium below the convection zone: such settling actually improves the agreement with helioseismology as was originally shown by Christensen-Dalsgaard, Proffitt & Thompson (1993). The impact of thermal diffusion on solar models has been studied with great care by Turcotte et al. (1998) who showed that, for some elements, it increases the settling velocity by as much as 50%.

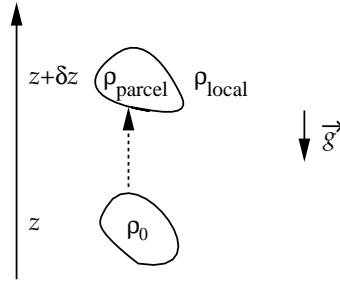


**Fig. 4.** As a fluid element is displaced upwards, it will become denser than its surroundings and will feel a downward restoring force if the Brunt-Väisälä frequency is positive, that is if the temperature gradient is smaller than the local adiabatic gradient.

Finally, diffusion can also have significant effects on the stellar structure when slow changes can accumulate over the stellar lifetime. In old population II stars, it is found to reduce the age determination by isochrones in globular clusters by about 10% (VandenBerg et al. 2002).

## 2 Rotational mixing

### 2.1 Introduction

Descriptions of rotational mixing have evolved a lot in recent years. The need for extra mixing in stars is widely recognized, and different rotational histories could well explain the variety of stellar behaviors.

Early descriptions have relied on very simple power laws relating the amount of mixing to the star's rotation rate (see *e.g.* Zahn 1983). In the case of lithium destruction in low mass stars for example, this would lead to larger dispersion in Li than observed (Schatzman & Baglin 1991).

Very early on, it was recognized that such scaling laws fail to produce an appropriate depth dependent diffusion profile and that consistent models must be built that take into account the angular momentum evolution (Endal & Sofia 1978). To do so, one must consider all possible transport processes for angular momentum and then analyze their effect on the transport of chemicals.

### 2.2 Rotation driven instabilities

In this first section, we will be looking at hydrodynamical instabilities. They are presented by considering what happens if one displaces a fluid parcel from its original position.

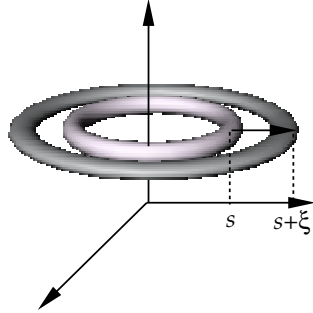


**Fig. 5.** To take into account the stabilizing effect of rotation, we expand a torus by an amount  $\xi$ .

### 2.2.1 Brunt-Väisälä frequency

Let us displace upwards a parcel of fluid from its equilibrium position in a radiative zone (Fig. 4). If the displacement over a distance  $\delta z$  is adiabatic and if pressure equilibrium is maintained, the density inside the parcel  $\rho_{\text{parcel}}$  will be larger than the local density  $\rho_{\text{local}}$  by an amount

$$\frac{\rho_{\text{parcel}} - \rho_{\text{local}}}{\rho_0} = \delta z \left( -\left. \frac{d \ln T}{dz} \right|_{\text{ad}} + \frac{d \ln T}{dz} \right) - \delta z \frac{d \ln \mu}{dz} = \frac{\delta z}{H_P} (\nabla_{\text{ad}} - \nabla + \nabla_{\mu}) \quad (2.1)$$

where  $H_P = -dz/d \ln P$  is the pressure scale height. We also used the classic notation of stellar modeling  $\nabla = d \ln T / d \ln P$ . The parcel then experiences a restoring force  $g(\rho_{\text{parcel}} - \rho_{\text{local}})$ , giving rise to an oscillation characterized by the Brunt-Väisälä frequency  $N$  defined as

$$N^2 = N_T^2 + N_{\mu}^2 = \frac{g}{H_P} (\nabla_{\text{ad}} - \nabla + \nabla_{\mu}). \quad (2.2)$$

The region is locally stable against convection if  $N^2$  is positive.

### 2.2.2 Solberg-Høiland instability

The next instability is related to the Coriolis force (Rayleigh 1916, Taylor 1923). We consider a fluid in *cylindrical rotation*. In the absence of gravity, pressure gradients balance centrifugal acceleration

$$-\frac{1}{\rho} \frac{dP}{ds} + s\Omega^2 = 0. \quad (2.3)$$

Let us displace a fluid torus over some distance  $\xi$  (Fig. 5). The net force acting on the fluid is proportional to the difference between the torus' angular momentum

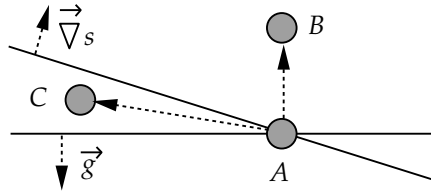


**Fig. 6.** In a baroclinic state, equipotentials and isentropic surfaces do not coincide. In a displacement from  $A$  to  $B$ , the local entropy rises, and this state is stable. However, in a displacement from  $A$  to  $C$ , the local entropy decreases, and this characterizes *baroclinic instabilities*.

$(s + \xi)\Omega_{\text{torus}}^2$  and the equilibrium value  $(s + \xi)\Omega_{s+\xi}^2$ . Since the Coriolis force ensures (specific) angular momentum ( $j = s^2\Omega$ ) conservation, it may be written as

$$(s + \xi)\Omega_{\text{torus}}^2 - (s + \xi)\Omega_{s+\xi}^2 = \frac{1}{(s + \xi)^3} (j_s^2 - j_{s+\xi}^2) \simeq \frac{1}{s^3} \frac{d(j^2)}{ds} \xi \quad (2.4)$$

valid to first order in  $\xi$ . We use this condition to define the Rayleigh frequency

$$N_{\Omega}^2 = \frac{1}{s^3} \frac{d}{ds} (s^2\Omega)^2 \quad (2.5)$$

which corresponds to a restoring force if positive, that is, if the specific angular momentum increases outward.

If gravity is taken into account, there are now two restoring forces. For equatorial radial displacements, the stability condition then reads

$$N^2 + N_{\Omega}^2 \geq 0. \quad (2.6)$$

For general axisymmetric perturbations, the stability criterion is twofold:

- Condition (2.6) must be satisfied;
- Specific angular momentum must increase from pole to equator.

The second condition corresponds to applying the Rayleigh criterion ( $N_{\Omega}^2 > 0$ ) to an isentropic surface; in the limit of no rotation, the first condition corresponds to the Schwarzschild criterion. These conditions have been derived by Solberg (1936) and Høiland (1941).

### 2.2.3 Baroclinicity

If the star's rotation state is not cylindrical, it can be shown that surfaces of constant pressure, density, entropy and gravity do not coincide<sup>5</sup>. This is called a

<sup>5</sup>Baroclinicity could also be caused by uneven heating (in a binary system) and this is the case in the Earth's atmosphere.

*baroclinic state* (in opposition to a *barotropic state*). Let us now imagine displacing a fluid element vertically<sup>6</sup> in such a star, going from  $A$  to  $B$  in Fig. 6. Assuming adiabaticity, the fluid will then be denser than its environment and gravity will restore it to its original position. However, if the same parcel is moved to  $C$ , it will now have a lower density, and gravity will make it rise, leading to an instability, which is called a *baroclinic instability*. However, angular momentum conservation makes axisymmetric movements towards  $C$  impossible (Knobloch & Spruit 1982). In the case of non-axisymmetric disturbances, fluid element exchange angular momentum (Cowling 1951), allowing instability, which gains energy by lowering the center of mass of the corresponding fluid.

These non-axisymmetric perturbations have been studied in the geophysical context using the  $\beta$ -plane approximation<sup>7</sup>. Knobloch & Spruit (1982) present a summary of these results, and conclude that instability is possible only for fast rotation that is if

$$N^2 < \left( \frac{d\Omega}{d \ln r} \right)^2. \quad (2.7)$$

## 2.2.4 GSF instability

In stellar interiors, thermal diffusivity  $K_T$  is much larger than viscosity  $\nu$  which controls angular momentum diffusion. This weakens the stabilizing effect of the density stratification (Goldreich & Schubert 1967, Fricke 1968). In the case of a vanishingly small viscosity, Goldreich & Schubert (1967) concluded that

... a necessary condition for stability is that the angular momentum per unit mass be an increasing function of distance from the rotation axis

which can also be expressed as

$$N_\Omega^2 \geq 0 \quad \text{and} \quad \frac{\partial \Omega}{\partial z} = 0, \quad (2.8)$$

which is similar to the Rayleigh criterion for incompressible, inviscid fluids (see *e.g.* Chandrasekhar 1961). This instability which depends on heat diffusion has a lower growth rate, and this changes the nature of the instability (it becomes “diffusive”). Indeed, for thermal diffusivity to be efficient, the length scale of the perturbation has to be small, and this reduces the efficiency of the instability.

Fricke (1968) and later Acheson (1978) considered the effect of a finite viscosity and presented a modified version of the Solberg-Høiland criterion for stability

$$\frac{\nu}{K_T} N_T^2 + N_\Omega^2 \geq 0 \quad (2.9)$$

<sup>6</sup>The vertical is defined by the direction of gravity.

<sup>7</sup>This approximation consist in a local study of the equations in a tangent plane touching the surface of the sphere at a given latitude. The Coriolis force is then expanded linearly around its local value  $\beta = 2\Omega \cos \theta$ .

together with

$$\left| s \frac{\partial \Omega}{\partial z} \right|^2 < \frac{\nu}{K_T} N_T^2, \quad (2.10)$$

permitting a small amount of differential rotation in  $z$  before instabilities set in.

### 2.2.5 ABCD instability

If the star is not chemically homogeneous, mean molecular weight gradients also contribute to the density stratification. Just like the restoring force associated with the temperature stratification is reduced by the thermal diffusivity, this contribution is also weakened, but this time by molecular diffusivity  $K_\mu$ . The Solberg-Høiland criterion is further modified and becomes

$$\frac{\nu}{K_T} N_T^2 + \frac{\nu}{K_\mu} N_\mu^2 + N_\Omega^2 \geq 0. \quad (2.11)$$

Since  $K_\mu$  is rather small (of the order of  $\nu$ ), this instability likely does not set in. There is however another possibility. When displacing a parcel towards  $C$ , it will come back to its equilibrium position  $A$  due to momentum conservation. However, if thermal diffusion is large enough, it will then be cooler than its surroundings, and the parcel will sink further in. This produces growing oscillations, a situation called *overstability*. The condition for stability is then (Knobloch & Spruit 1983)

$$\frac{\nu}{K_T} (N_T^2 + N_\mu^2) + N_\Omega^2 \geq 0. \quad (2.12)$$

All criteria described so far are linear, and little work has been done on the non-linear behavior of the corresponding instabilities, implying that we do not know how efficient they are for mixing.

## 2.3 Shear instability

Rayleigh (1880) derived a linear stability criterion against shear, which reads simply

$$\frac{d^2 u}{dr^2} = 0 \quad (2.13)$$

everywhere, or in words, there must be no inflection point in the velocity profile for it to be stable. In experimental cases however, it is known that turbulence can develop even in the absence of such an inflection point (that was shown for example by Wendt (1933) in the study of the flow between two cylinders). This instability is linked to the presence of *finite amplitude* fluctuations that can appear in the fluid.

To look into the non-linear regime of interest, we can study the energetics of the problem. It can be shown that the minimum energy state of a rotating fluid is solid body rotation. Thus, if the star is rotating differentially, by homogenizing the velocities, it is possible to extract energy. However, to do so, one must be

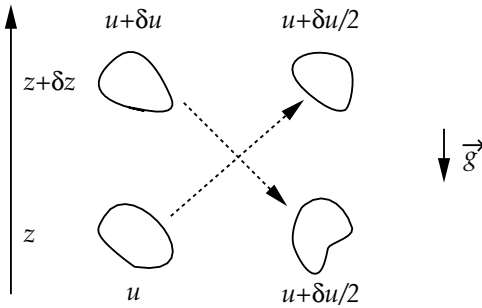


**Fig. 7.** To derive the instability condition against shear, let us take a blob at level  $z$  with a velocity  $u$  and move it upward to the level  $z + \delta z$ . Simultaneously, we take a blob at level  $z + \delta z$  with a velocity  $u + \delta u$  and move it down. When doing so, we also homogenize the velocities that become  $u + \delta u/2$  for both blobs. We gain  $1/4\rho\delta u^2$  in kinetic energy, but lose  $g\Delta\rho\delta z$  in work against gravity. This leads to the Richardson criterion.

able to overcome the density stratification. By comparing both and assuming adiabaticity, one obtains the Richardson instability criterion (Fig. 7)

$$Ri \equiv \frac{N^2}{(du/dz)^2} < Ri_{\text{crit}} = \frac{1}{4} \quad (2.14)$$

(see *e.g.* Chandrasekhar 1961). This becomes our *non-linear* condition for instability.

### 2.3.1 Dynamical shear instability

Along isobars, there is no restoring force, and thus, shear is unstable as soon as horizontal differential rotation is present. Horizontal shear is thus a dynamical instability, acting on a dynamical hence quite short time-scale and leading to a large horizontal turbulent viscosity. A few attempts have been made in order to evaluate this value (*e.g.* Richard & Zahn 1999, Maeder 2003, Mathis, Palacios & Zahn 2004), but as of now, there is no reason to prefer one formulation over the other. It has strong implications on the transport of elements and we will discuss these in § 2.4.4 and 2.6 (this is also discussed at length in Talon, Richard & Michaud 2005).

### 2.3.2 Secular shear instability

In the direction of entropy stratification, both the thermal and the mean molecular weight stratifications hinder the growth of the instability. However, thermal diffusion and horizontal shear act as to reduce the stabilizing effect of the stratification, just as in the case of the GSF instability (§ 2.2.4). We obtain the *instability*

criterion

$$\left(\frac{\Gamma}{\Gamma+1}\right) N_T^2 + \left(\frac{\Gamma_\mu}{\Gamma_\mu+1}\right) N_\mu^2 < Ri_{\text{crit}} \left(\frac{du}{dz}\right)^2 \quad (2.15)$$

where  $\Gamma = v\ell/K_T$  and  $\Gamma_\mu = v\ell/K_\mu$  (Talon & Zahn 1997, see also Maeder 1995). We normally use  $Ri_{\text{crit}} = 1/4$ , but this is open to discussion (see *e.g.* Canuto 1998). This criterion implies that, the smaller the eddy, the more efficient thermal diffusivity. In fact, there always exists an eddy that is small enough so that the instability criterion (2.15) will be satisfied. Turbulent diffusivity corresponds to the largest eddy satisfying (2.15); this is a non-linear description, based on energy considerations. It is the formulation we shall adopt to describe the vertical shear instability.

#### 2.4 Meridional circulation

The Eddington-Sweet meridional circulation is related to the thermal imbalance that is in general present in rotating stars. This imbalance was first pointed out by von Zeipel (1924) when he tried to describe thermal equilibrium in a rotating star in solid body rotation. Since such a star is barotropic, equi-potentials and iso-therms coincide, and are ellipsoids. When writing the divergence of the heat flux

$$-\nabla \cdot \vec{F} = \nabla \cdot (\chi \nabla T) = -\rho\varepsilon, \quad (2.16)$$

von Zeipel realized that, while the (horizontal) average of  $\nabla \cdot \vec{F}$  may equilibrate the energy generation  $\rho\varepsilon$ , it is not the case along an equipotential, except if this energy generation has a very special behavior, which is not realistic (this divergence is shown on the left of Fig. 8, in the case  $\varepsilon = 0$ ), and this became known as *von Zeipel's paradox*. Vogt (1925) and Eddington (1925) found a simple solution to the problem, which consists in considering the advection of entropy  $S$  in the heat equation

$$\rho T \vec{u} \cdot \vec{\nabla} S = \vec{\nabla} \cdot (\chi \vec{\nabla} T) + \rho\varepsilon, \quad (2.17)$$

where  $\vec{u}$  is the meridional circulation velocity, which is calculated with the above equality. This was done initially for the case of solid body rotation by Sweet (1950) and yields a large scale circulation that rises at the pole and sinks at the equator.

Sweet's solution is however not fully consistent since this large scale circulation advects angular momentum as well as entropy. This will modify the rotation profile, and hence feedback must be treated. Since this is actually (at least) a 2-D effect, not much progress has been made in incorporating it into stellar evolution codes until quite recently.

In a first step, models were built by treating the advection of momentum as a purely diffusive process (Endal & Sofia 1976, 1978, Pinsonneault et al. 1989, Langer 1991, these codes are still in use).

The key ingredient to allow the modeling of meridional circulation as a 1-D process is the assumption of highly anisotropic turbulence, with the vertical turbulent viscosity  $\nu_v$  being much smaller than the horizontal turbulent viscosity

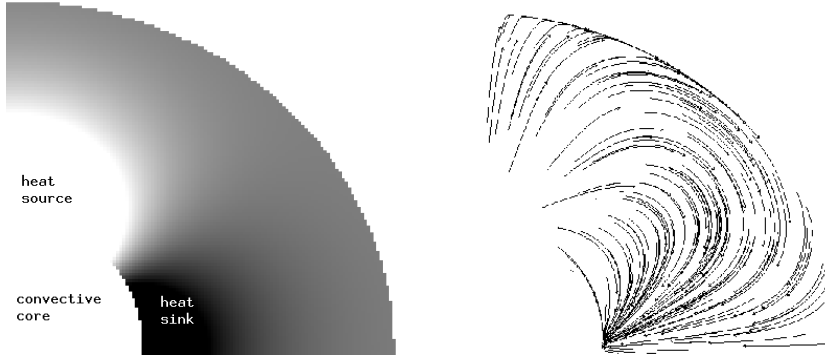


**Fig. 8.** The traditional approach to meridional circulation consists of calculating the thermal imbalance for a given rotation state (left, here in the case of solid body rotation with an oblateness of 10%) and evaluating the advective flux required to counter-balance this imbalance (right).

$\nu_h$ . This property is related to the vertical stratification (Tassoul & Tassoul 1983, Zahn 1992) and permits to assume a state of shellular rotation<sup>8</sup>, *i.e.*  $\Omega = \Omega(P)$ . Conditions for this approximation to be valid are discussed by Tassoul & Tassoul (1983), Zahn (1992) and Charbonneau (1992 - this discussion is based on numerical simulations).

#### 2.4.1 Heat flux

Under that assumption, and to first order, it is possible to derive an equation for the thermal imbalance in a star with a given (shellular) rotation profile. Then, as in the case of solid body rotation, meridional circulation is obtained by stating that advection of entropy  $S$  must neutralize this thermal imbalance

$$\rho T \vec{u} \cdot \vec{\nabla} S = \vec{\nabla} \cdot (\chi \vec{\nabla} T) + \rho \varepsilon - \vec{\nabla} \cdot \vec{F}_h \quad (2.18)$$

(this form of the equation also contains a turbulent horizontal heat flux  $\vec{F}_h$ , Maeder & Zahn 1998). The vertical component of the asymptotic circulation velocity is then

$$u = \frac{P}{\rho g C_P T} \frac{1}{(\nabla_{\text{ad}} - \nabla + \nabla_{\mu})} \left[ \frac{L}{M} (E_{\Omega} + E_{\Theta} + E_{\mu}) + \frac{TC_P}{\delta} \frac{\partial \Theta}{\partial t} \right] P_2(\cos \theta) \quad (2.19)$$

<sup>8</sup>Note that, in the case of shellular rotation equi-potentials do not exist, and will be replaced by isobars.

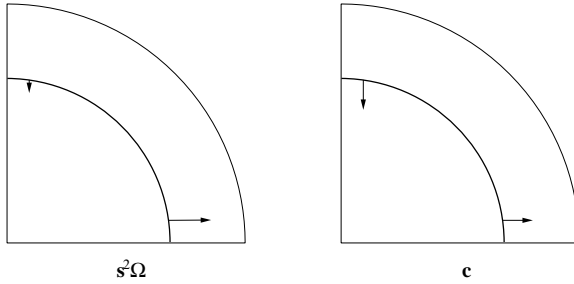


**Fig. 9.** Meridional circulation has a different effect on angular momentum and on chemicals. Even when horizontal mixing is strong, the large scale circulation produces a net flux of  $s^2\Omega$ , while there is no net flux of concentration. In fact, the evolution of  $c$  is possible only in the presence of horizontal inhomogeneities. (From Talon 1997).

(see Maeder & Zahn 1998 for the complete expression). The circulation velocity is related to a term  $E_\Omega$  which depends on the rotation rate, a term  $E_\Theta$  which depends on the radial differential rotation ( $\Theta \propto d\Omega^2/dr$ ) and a term  $E_\mu$  which depends on the horizontal variations of the mean molecular weight  $\mu$ . In a homogeneous solid body rotating star, only the first term survives, and one gets Sweet's (1950) classical solution characterized by a large circulation cell rising along the pole, with a reversed cell at the surface (Gratton 1945, Öpik 1951).

Let us note that if convective overshooting is not present, the solution diverges at the convective boundary where  $\nabla_{\text{ad}} - \nabla = 0$  and viscous boundary layers are then required (Tassoul & Tassoul 1982).

#### 2.4.2 Angular momentum transport

If the only transport processes present are meridional circulation and hydrodynamical instabilities, the distribution of angular momentum within the star will evolve according to an advection-diffusion equation

$$\rho \frac{d}{dt} [r^2\Omega] = \frac{1}{5r^2} \frac{\partial}{\partial r} [\rho r^4 \Omega u] + \frac{1}{r^4} \frac{\partial}{\partial r} \left[ \rho \nu_v r^4 \frac{\partial \Omega}{\partial r} \right] \quad (2.20)$$

(see Zahn 1992 for details). Note that the first term of this equation still corresponds to an advective process since, even if  $\Omega$  is homogeneous on isobars,  $s^2\Omega$  is not (see also Fig. 9). This will not be the case for chemicals (see § 2.4.4). Here we use a vertical turbulent viscosity  $\nu_v$  which is attributed to relevant rotational instabilities detailed in § 2.2 and 2.3.2. Neglecting the star's evolution, this equation admits a stationary solution in which advective transport is counterbalanced by turbulent transport. If no turbulence is present and if the star is homogeneous, circulation will simply stop, resulting in a rotation profile with a core rotating about 20% faster than the surface (Urpin et al. 1996, Talon et al. 1997, see also

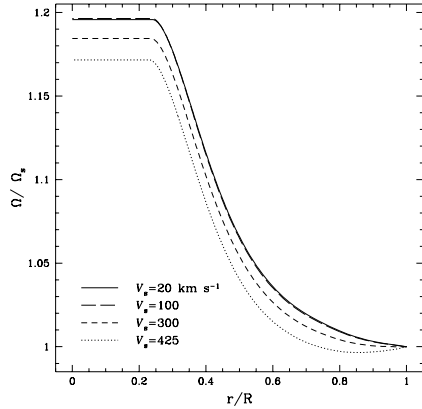


**Fig. 10.** Equilibrium rotation profile as given by Eq. (2.20) for various surface velocities in a  $9 M_\odot$  main sequence star. (Figure 1 from Talon et al. 1997.)

Fig. 10). The equilibrium profile in  $\Theta$  thus depends on the nature and the vigor of rotational instabilities present in the star. However, when using realistic values for  $\nu_v$ , it varies only slightly, and so, meridional circulation is in general much weaker than predicted by the simple Eddington-Sweet solution. For any rotation profile, the direction of the circulation can be deduced from the requirement of reconstructing this equilibrium solution.

If the star is not chemically homogeneous, meridional circulation will produce horizontal variations of mean molecular weight  $\mu$  out of the vertical chemical stratification. These contribute to the heat flux, via the equation of state. Equation (2.19) shows that, if horizontal variations of mean molecular weight are present, the equilibrium profile described in the previous paragraph exists; however, it now describes the function  $\Theta - \tilde{\mu}/\mu$  ( $\tilde{\mu}$  refers to the horizontal fluctuation of  $\mu$ ). If rotation evolves solely under the action of meridional circulation and turbulence, this equilibrium requires an increase in differential rotation (compared to the homogeneous case) in order to maintain the asymptotic solution. This effect has been observed in fully consistent unidimensional calculations including differential rotation and mean molecular weight gradients (Talon et al. 1997, Palacios et al. 2003).

If the star is constrained to rotate as a solid body<sup>9</sup> and does not evolve, the build up of horizontal mean molecular weight fluctuations can thus also lead to a circulation free state, as originally suggested by Mestel (1953).

In an evolving stellar model, the required equilibrium profile also evolves (*e.g.* Talon et al. 1997). This leads to the appearance of a “re-adjustment” circulation, which is added to the asymptotic circulation. This circulation cannot be avoided, even in chemically inhomogeneous stars rotating as solid bodies.

<sup>9</sup>In solid body rotation, no hydrodynamical instabilities can develop.

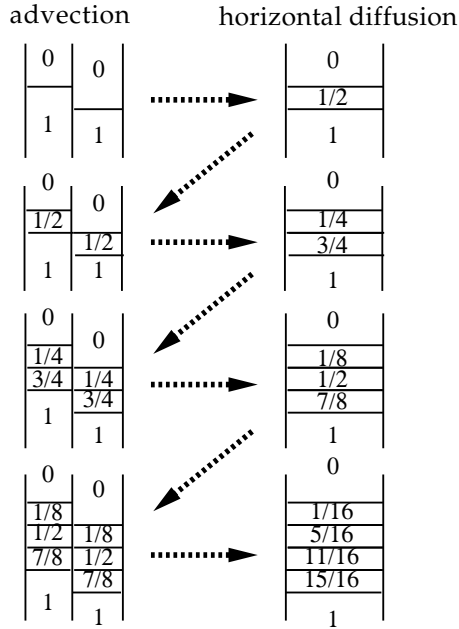


**Fig. 11.** The combination of advection and horizontal transport leads to an effective vertical diffusion. In this cartoon, we are slowly building a discrete version of the error function, characteristic of a diffusion process.

#### 2.4.3 Wind-driven circulation

If the star’s surface is braked via a magnetic torque, as is the case of Pop I stars cooler than about 7000 K, the internal distribution of angular momentum is rapidly moved away from its equilibrium profile, with large shears developing in the outer regions. This is the regime of “wind-driven” circulation, and the model presented up to now predicts strong mixing related to such a state.

#### 2.4.4 Chemical transport

While momentum transport remains a truly advective process when considering the combined effect of meridional circulation and horizontal diffusion, it is possible to understand heuristically that this combination leads to (vertical) diffusion in the case of chemicals (Fig. 11, see also Chaboyer & Zahn 1992; this has also been shown in numerical simulations by Charbonneau 1992). This is the case because horizontal turbulence continually reduces horizontal chemical inhomogeneities, impeding efficient advection. This effect is felt as soon as

$$D_h > |rU| \quad \text{and} \quad D_h/D_v \gtrsim 1000 \quad (2.21)$$

(Charbonneau 1992). In the following, we assume that diffusion coefficients are equal to the turbulent viscosities *i.e.*  $D_v = \nu_v$  and  $D_h = \nu_h$ . The advection + horizontal diffusion + vertical diffusion equation can then be replaced by a purely diffusive equation, with vertical turbulent transport and an effective diffusivity depending on horizontal turbulent transport  $D_h$  and advective velocity  $u$

$$\rho \frac{dc}{dt} = \rho \dot{c} + \frac{1}{r^2} \frac{\partial}{\partial r} [r^2 \rho V_{ip} c] + \frac{1}{r^2} \frac{\partial}{\partial r} \left[ r^2 \rho (D_{\text{eff}} + D_v) \frac{\partial c}{\partial r} \right]. \quad (2.22)$$

The effective diffusivity is  $D_{\text{eff}} = r^2 u^2 / (30 D_h)$  (Chaboyer & Zahn 1992);  $\dot{c}$  is the nuclear production/destruction rate of the species, and  $V_{ip}$  is the atomic diffusion velocity (see § 1).

### 2.5 Some applications of rotational mixing

This theory of rotational mixing based on an advective formulation of meridional circulation and shear instabilities has been applied to a wide variety of stars. In the case of massive stars, extensive studies have been conducted by the Geneva group, with great success in explaining problems such as:

- He and N overabundances in O- and early B-type stars and in super-giants;
- the number ratio of red to blue super-giants;
- the Wolf-Rayet to O-type stars ratio.

Recent results regarding massive stars are given in Meynet (2007, this volume).

In the case of low mass stars, rotational mixing has been applied to the case of the lithium dip<sup>10</sup>. In this model, the hot side of the lithium dip corresponds to stars that suffer magnetic braking (see § 2.4.3 and 3.4); this induces large internal differential rotation, increasing rotational mixing and thus, surface lithium depletion. Rotational mixing reproduces well the hot side of the dip (Talon & Charbonnel 1998, Palacios et al. 2003, Fig. 12) but fails for temperatures below  $T_{\text{eff}} \lesssim 6700$  K.

Rotational mixing has also been applied to the study of the solar rotation profile. According to helioseismology, the solar radiative zone is rotating more or less as a solid body (see *e.g.* Chaplin et al. 1999, Couvidat et al. 2003). In that case, complete self-consistent calculations predict that radial differential rotation remains large at the solar age (see Fig. 13). This was shown independently by two groups, using slightly different approaches to rotational mixing<sup>11</sup> and three different stellar evolution codes (Pinsonneault et al. 1989, Chaboyer et al. 1995, Talon 1997, Matias & Zahn 1998).

<sup>10</sup>The so-called lithium dip, discovered by Boesgaard & Tripicco (1986) and observed in all galactic clusters older than  $\approx 300$  Myr, refers to a strong lithium depletion in a narrow region of  $\approx 300$  K in effective temperature, centered around  $T_{\text{eff}} \approx 6700$  K. Lithium is burned at a temperature of  $\sim 2.5 \times 10^6$  K, which, in these stars, is located well into the radiative zone. As one looks at cooler stars, this burning layer is located closer to the base of the convective envelope.

<sup>11</sup>The Yale group uses a diffusive approximation for the meridional circulation instead of the formulation given in these notes.

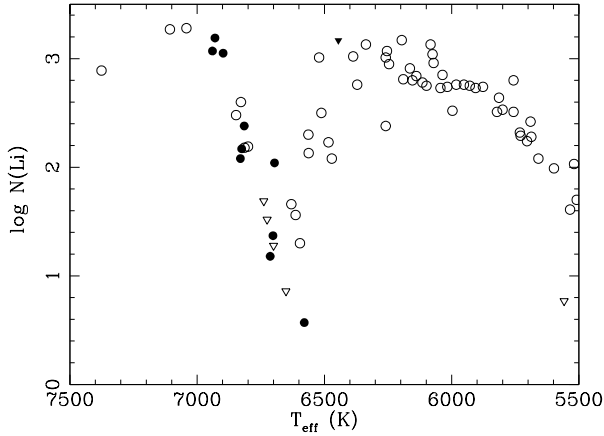


**Fig. 12.** Predicted (closed circles) and observed (open circles; inverted open triangles are upper limits) lithium abundances in the Hyades around the lithium dip. Theoretical models are made with initial velocities of 50, 100 and 150  $\text{km s}^{-1}$ , and final velocities corresponding to those measured in the Hyades for the corresponding effective temperature. For cooler stars, lithium depletion remains large ( $N(\text{Li})$  is too small), at a level incompatible with observations. The inverted filled triangle corresponds to the prediction of rotational mixing if the inner rotation profile is artificially assumed to be solid body rotation, with surface braking. (Adapted from Fig. 6 of Talon & Charbonnel 1998.)

These results on low-mass stars indicate that there must be another efficient transport process for angular momentum active when the surface convection zone appears; this would explain both the solar rotation profile and the rise of the lithium abundance on the cool side of the dip (Talon & Charbonnel 1998).

## 2.6 Open problems in rotational mixing

The 1-D modeling of meridional circulation is certainly a very important step in understanding and testing models of stellar evolution with rotation. However, one must not forget that it is actually an advective transport and that unidimensional modeling remains an approximation.

The major limitation of the model comes from the invoked horizontal turbulent diffusion coefficient  $D_h$ . While in actual models it is linked to the source of horizontal shear (that is, some function of  $u$ ) its magnitude remains quite uncertain. Furthermore, the hypothesis is that its effect will be to smooth out horizontal fluctuations. This is the case in the Earth's atmosphere albeit only up to scales

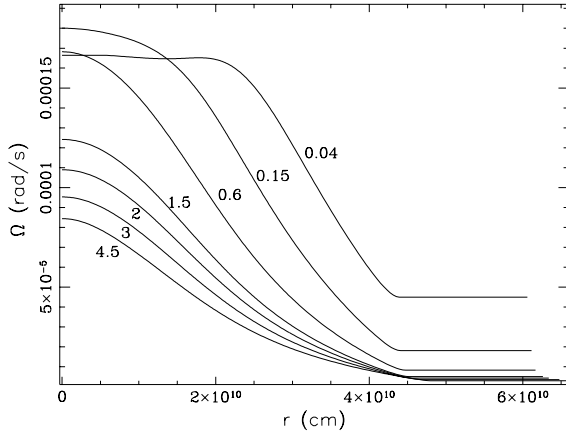


**Fig. 13.** Evolution of the solar rotation profile under the effect of rotational mixing only. The initial rotation velocity is assumed to be  $100 \text{ km s}^{-1}$ , and labels indicate the age in Gyr. (Figure 11.1 from Talon 1997.)

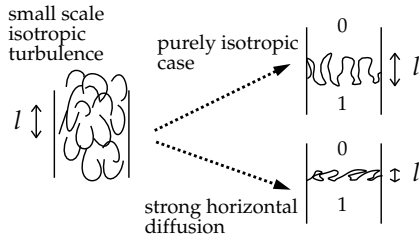


**Fig. 14.** Strongly anisotropic turbulence reduces the vertical extent of eddies, leading to a reduction of vertical transport.

that are smaller than the Rossby radius<sup>12</sup>, which is given by

$$L_{\text{Rossby}} = \frac{H_P N}{2\Omega \sin \theta} \quad (2.23)$$

where  $\theta$  is the latitude. With typical values for  $H_P$  and  $N$ , it is of order  $L_{\text{Rossby}} \simeq (50R)/(v_{\text{rot}} \sin \theta)$ , with  $v_{\text{rot}}$  in  $\text{km s}^{-1}$ . This limit will thus become relevant for stars rotating faster than about  $100 \text{ km s}^{-1}$ .

Another issue concerns the vertical transport of chemicals in the presence of strongly anisotropic turbulence. As a turbulent eddy is displaced vertically in the fluid, it loses some of its coherence by being mixed by horizontal turbulence (see Fig. 14). This effect has been demonstrated in numerical simulations (Vincent

<sup>12</sup>This scale is the one at which Coriolis' force becomes comparable to vertical stratification.

et al. 1996, Toqué et al. 2006). Talon, Richard & Michaud (2006) invoked such erosion in the context of AmFm stars. In § 1.5, we mentioned that AmFm stars can be understood as the result of radiative accelerations. However, there is a need for a competing process to reduce the magnitude of over/underabundances predicted in the case of a perfectly stable envelope. When rotational mixing prescriptions as described here are applied to such stars, the associated vertical transport of elements is too strong to account for AmFm stars; a reduction of the vertical transport by horizontal turbulence is required to correctly reproduce the observed abundances (Talon et al. 2006). However, such a reduction would degrade the good agreement obtained in the case of massive stars. Also, the effect of such anisotropic turbulence on a non-passive component (*e.g.* angular momentum) remains to be studied.

A better understanding of the interaction between meridional circulation and turbulent properties could be obtained via the resolution of the full Navier-Stokes equations of hydrodynamics in 3-D (see also the 2-D, steady, calculations by Garaud 2002). This is a numerical challenge, as many time-scales are involved in the problem. A first step was taken in that direction by Talon et al. (2003) who wrote a code to tackle that problem. Used in direct numerical simulations with unrealistically large viscosities, it does lead to stationary solutions. A comparison of these solutions with those of analytical models should permit a verification of their validity in the limit of large viscosities. The goal is then to reduce the viscosities and introduce a sub-scale turbulence model in order to represent unresolved features and to examine how solutions are modified.

### 3 Magnetic fields

#### 3.1 Introduction

There is a strong connection between rotation and magnetic fields. To examine that relation, let us start by taking a quick look at the equations that govern this interaction. We first have the induction equation

$$\frac{\partial \vec{B}}{\partial t} = \nabla \times (\vec{U} \times \vec{B} - \eta \nabla \times \vec{B}), \quad (3.1)$$

which describes the action of a velocity field  $\vec{U}$  on the magnetic field  $\vec{B}$  in the presence of magnetic diffusivity  $\eta$ . This equation is obtained by a combination of Ampère's law in the limit of no electric field and of Faraday's law of induction. We must also consider the momentum equation which takes into account the magnetic field by the means of the Lorentz force

$$\frac{\partial \vec{U}}{\partial t} + (\vec{U} \cdot \nabla) \vec{U} = -\frac{1}{\rho} \nabla P + \frac{1}{4\pi\rho} (\nabla \times \vec{B}) \times \vec{B} + \vec{g}. \quad (3.2)$$

The relative importance of magnetic field compared to inertial forces is given by the magnetic Reynolds number  $\text{Re}_m$

$$\text{Re}_m = \frac{ud}{\eta} \quad (3.3)$$

where  $u$  and  $d$  are respectively typical velocity and length scales. The “stretching” of field lines is efficient when this number is large.

Here, we will discuss some of the impacts of magnetic fields on stellar structure, with special focus on their interaction with rotation.

### 3.2 Ferraro's law of isorotation

Probably the best known effect of magnetic fields is to produce solid body rotation: this is a restatement of Ferraro's theorem (1937), which we will examine here. To derive this theorem, we first separate our magnetic field into poloidal and toroidal components

$$\vec{B} = \vec{B}_p + B_\phi \vec{e}_\phi \quad (3.4)$$

with  $\vec{e}_\phi$  a unit vector in the  $\phi$  direction. We now make various assumptions:

- the fluid is perfectly conducting ( $\eta = 0$ );
- the fluid is incompressible ( $\nabla \cdot \vec{U} = 0$ );
- the solution is axisymmetric;
- there is no meridional velocity field;
- the solution is stationary.

The induction equation for the  $B_\phi$  component then reads

$$\begin{aligned} \frac{\partial B_\phi}{\partial t} &= [\nabla \times (\vec{U} \times \vec{B})] \cdot \vec{e}_\phi \\ &= [\vec{U} (\nabla \cdot \vec{B}) - \vec{B} (\nabla \cdot \vec{U}) + (\vec{B} \cdot \nabla) \vec{U} - (\vec{U} \cdot \nabla) \vec{B}] \cdot \vec{e}_\phi \\ &= [(\vec{B}_p \cdot \nabla) U_\phi \vec{e}_\phi - (U_\phi \vec{e}_\phi \cdot \nabla) \vec{B}] \cdot \vec{e}_\phi \end{aligned} \quad (3.5)$$

This equation shows how differential rotation produces a toroidal field from a purely poloidal field. In order to obtain a stationary state, we require

$$(\vec{B}_p \cdot \nabla) \Omega = 0 \quad (3.6)$$

with  $U_\phi = r \sin \theta \Omega$ . This equation indicates that, under equilibrium conditions, fluid parcels that are located along the same poloidal field line must have the same angular velocity.

### 3.3 Alfvén speed

It is not sufficient to know what the equilibrium state is, one must also evaluate the timescale required to reach this equilibrium. Here, we want to know how a

field line, that is stretched perpendicularly, responds. This gives rise to an Alfvén wave, and the speed of this propagation is thus the Alfvén speed  $v_A$ <sup>13</sup>

$$v_A = B_0 (4\pi\rho)^{-1/2} \quad (3.7)$$

(Alfvén 1942). In the star, shear will propagate over a stellar radius  $R$  in an Alfvén time

$$\tau_A = \frac{R}{v_A} \quad (3.8)$$

which also defines the Alfvén frequency

$$\omega_A = \frac{1}{\tau_A} = \frac{v_A}{R}. \quad (3.9)$$

Let us mention that, in the absence of dissipation, this shear will simply bounce back and forth, and iso-rotation along poloidal field lines would not be obtained (see e.g. Mestel & Weiss 1987). Furthermore, in order to reach solid body rotation, diffusion is also required to “connect” the fluid velocity between various field lines. These two effects contribute to a significant increase of the timescale required to actually reach solid body rotation.

### 3.4 Solar spin-down

We already mentioned in § 2.4.3 the problem of magnetic braking that is observed in all stars that have a “significant” surface convection zone, in practice all stars cooler than  $T_{\text{eff}} \lesssim 7000$  K. This can be understood in terms of mass loss in a magnetized wind, as originally suggested by Schatzman (1962) and Weber & Davis (1967): it is related to the fact that, when magnetic energy is larger than the wind’s kinetic energy, matter is bound to co-rotate with the star even at large distances, leading to a large angular momentum loss even for a modest mass loss. An order of magnitude calculation is as follows. The surface solar dipolar field is

$$B_{0r} \approx 1 \text{ G}. \quad (3.10)$$

Magnetic flux conservation imposes

$$r^2 B_r = R_\odot^2 B_{0r} \quad (3.11)$$

while mass conservation leads to

$$\rho u_r r^2 = \rho_0 u_{0r} R_\odot^2 \quad (3.12)$$

where  $u_r$  is the radial velocity in the wind for the mass loss. The comparison of the kinetic energy to the magnetic energy is given by the Alfvénic Mach number

$$M_A^2 = \frac{4\pi\rho u_r^2}{B_r^2} = \frac{1}{\rho} \frac{4\pi\rho_0^2 u_{0r}^2}{B_{0r}^2} \equiv \frac{\rho_A}{\rho} \quad (3.13)$$

---

<sup>13</sup>This velocity is obtained by coupling linearized versions of Eqs. (3.1) and (3.2).

which we use to define the Alfvén density  $\rho_A$ , corresponding to the density at which  $M_A = 1$ . If the mass loss velocity  $u_{0r}$  is known, one can evaluate this density. Using the values at the Earth orbit,  $u_E \simeq 400 \text{ km s}^{-1}$  and  $\rho_E \simeq 12 \times 10^{-24} \text{ g cm}^{-3}$  leads to a density of

$$\rho_A \simeq 5 \times 10^{-21} \text{ g cm}^{-3}. \quad (3.14)$$

Building a steady wind model similar to Parker’s (1960), Weber & Davis (1967) concluded that the corresponding Alfvén radius is

$$r_A \simeq 24R_\odot. \quad (3.15)$$

The wind must co-rotate with the magnetic field up to that distance, explaining the efficiency of the surface braking. A more complete description of this process which also discusses the role of various field configurations is given by Kawaler (1988, see also references therein). This produces surface braking of the star. Through convective motions, it is expected that this braking affects the whole convection zone. The problem of the transport of angular momentum in the radiative zone remains.

### 3.5 The solar rotation

Another interesting application of Ferraro’s law lies in the spin down of the solar radiative zone. As already mentioned (§ 2.5), helioseismology concludes that the the Sun’s deep interior is rotating more or less rigidly, and rotational mixing alone is not able to provide an explanation of this feature. An obvious solution to this problem is to invoke a fossil magnetic field, as described at length by Mestel & Weiss (1987). Charbonneau & MacGregor (1993, see also Barnes, Charbonneau, & MacGregor 1999) studied this effect in a 2-D solar model, assuming a *fixed* poloidal configuration. They applied surface braking to a star originally rotating at  $50 \Omega_\odot$ . In these simulations, as the surface is spun-down, the poloidal field is sheared; this builds up a toroidal field that will then, through the Lorentz force, oppose the shear. This toroidal field grows until the torque exerted by magnetic stresses

$$\tau = r^3 \langle B_r B_\phi \rangle \quad (3.16)$$

is strong enough to oppose the wind-mediated torque. At this stage, the core and the envelope fully couple, and spin-down together, with the overall differential rotation remaining small. This occurs for all values of the poloidal field, although the time-scale for this re-coupling to occur depends on  $B_r$ . Several configurations have been tested for the poloidal field, with the field lines anchored in the convection zone (configurations D1 and D2 of their models), or not (configuration D4) or barely touching (configuration D3).

Initial calculations were performed with the convection zone rotating as a solid body. When latitudinal differential rotation in the convection zone is present, due to Ferraro’s law, it imprints itself in the interior (MacGregor & Charbonneau 1999). Agreement with helioseismic inversion require that the field be totally contained in the radiative zone (configuration D4).

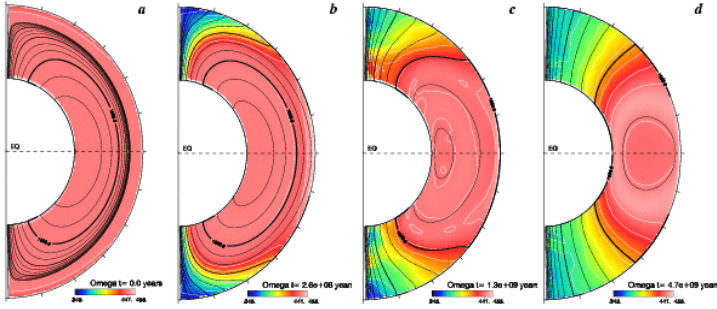


**Fig. 15.** Temporal evolution, in a 3-D MHD model of the solar radiative zone, of the angular velocity  $\Omega$  (color contours and white lines) and the mean axisymmetric poloidal field (superimposed black lines), which initially is buried deeply in the interior (Fig. 4 of Brun & Zahn 2006). **a-d)** sequence spanning 4.7 Gyr (in solar equivalent units) of the dipolar magnetic field in the presence of rotation and shear. The field lines gradually connect with the imposed top shear, thereby enforcing differential rotation at all depths above latitudes greater than  $\approx 40^\circ$ , at the (equivalent) age of the Sun. Note also in frames **c-d** the distortion near the poles of the lines of constant  $\Omega$ , which is associated with the Taylor instability (see § 3.7).

Recent 3-D MHD numerical simulations in which the fossil poloidal field is allowed to evolve have been performed to study this mechanism in a fully consistent way, using the ASH code (Brun & Zahn 2006 and references therein). In all cases studied by these authors, the fossil field is found to diffuse outwards and inexorably connects with the outer convection zone, imprinting its differential rotation to the radiative interior. Contrary to the expectation of Gough & McIntyre (1998), the meridional flow that develops between the base of the convection zone and the dipole poloidal field is not able to stop its progression. It remains to be seen whether things would change if lower (more realistic) values of the magnetic diffusivity, thermal diffusivity and viscosity were used (this is currently out of reach numerically).

### 3.6 Magnetic stability

Another issue that needs concern stellar astrophysicists regarding magnetic fields is that of the magnetic stability. This is well illustrated by the following quote from Braithwaite & Spruit (2004):

“Although there have been educated guesses as to what shape a field in a stable equilibrium might have, all configurations studied with the analytic methods available so far were found to be unstable on the Alfvén timescale; it has been impossible to prove stability for even a single field configuration.”

However, while the presence of a large scale magnetic field in the solar radiative zone remains unproven, such fields are actually measured in several stars, as *e.g.* in Ap stars. Braithwaite & Spruit made numerical simulations of such stars, in order to understand what the structure of their field should look like. In their 3-D simulation, they model a non-rotating  $n = 3$  polytrope, in which they introduced an initial random magnetic field. The total energy  $E_B$  in that initial field is assumed rather small, that is  $E_B \approx 0.01E_T$ , with  $E_T$  the thermal energy of the star.

They found that, after a few Alfvén times, it was indeed possible to find a stable magnetic structure, which has the following properties:

- the field is approximately axisymmetric;
- the poloidal field has the same amplitude as the toroidal field;
- magnetic helicity is conserved.

The properties of their magnetic field are in close agreement with those actually measured in Ap stars, giving strength to the idea that it is of fossil rather than dynamo origin.

### 3.7 The Tayler-Spruit instability

The issue of magnetic stability in rotating stars has been studied theoretically in great details by several authors, and an extensive review of these can be found in Tayler (1973) and Pitts & Tayler (1985). These linear stability study are performed using perturbations of the equations for the conservation of mass, momentum (Eq. 3.2) and energy and the magnetic induction equation (Eq. 3.1) and verifying whether a lower energy state exists. Actual calculations are time consuming, and have to be made for each magnetic configuration. The relative efficiency of these instabilities was reexamined by Spruit (1999), and he concluded that, the *pinch-type instability*, which is now more widely known as the *Tayler-Spruit instability* in the stellar community, was the first to set in. We will review this process here.

Starting from a seed poloidal field  $B_r$ , differential rotation winds it up and generates a mainly azimuthal field  $B_\phi \gg B_r$ . The most unstable mode for this horizontal field is then a non-axisymmetric “kink” mode, in which the displacement is mainly horizontal (to minimize work against the density stratification) and incompressible (to minimize work against pressure) (see Fig. 16). Together, these two conditions imply

$$l_h/l_r \approx \xi_h/\xi_r \gg 1 \quad (3.17)$$

where  $l_h$  and  $l_r$  are respectively the horizontal and vertical length scales and  $\xi_h$  and  $\xi_r$  are the horizontal and vertical displacements. Ignoring thermal diffusivity, the work against buoyancy is

$$W = \frac{1}{2} \rho \xi_r^2 N^2 \quad (3.18)$$

while the kinetic energy of the displacement is

$$K = \frac{1}{2} \rho \xi^2 \omega_A^2 \simeq \frac{1}{2} \rho \xi_h^2 \omega_A^2 \quad (3.19)$$

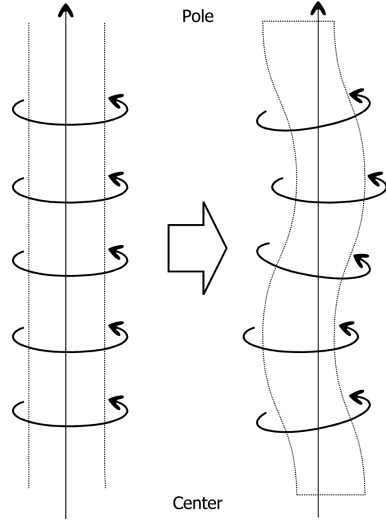


**Fig. 16.** In the kink instability, toroidal field loops around the rotation axis move (mostly horizontally) relative to each other. Adapted from Tayler (1973).

which yields the instability condition

$$l_r < \frac{r\omega_A}{N} \quad (3.20)$$

assuming  $l_h \simeq r$ . This limits the vertical amplitude of the instability. However, magnetic diffusivity damps those small scales. The characteristic time-scale for magnetic diffusion  $t_d = l_r^2/\eta$  has to be larger than the growth time of the instability which, in the limit of strong Coriolis force is of order

$$\sigma_B = \omega_A^2/\Omega, \quad (3.21)$$

for the instability to experience a net growth. One finds another condition for the vertical scale

$$l_r^2 > \frac{\eta\Omega}{\omega_A^2}. \quad (3.22)$$

The combination of these two conditions yields a criterion for magnetic instability

$$\frac{\omega_A}{\Omega} > \left(\frac{N}{\Omega}\right)^{1/2} \left(\frac{\eta}{r^2\Omega}\right)^{1/4}. \quad (3.23)$$

This condition, valid in the limit of zero thermal diffusivity  $K_T$ , was originally derived by Acheson (1978). It would correspond to a region where  $N$  is dominated by mean molecular weight gradients. When  $K_T$  is taken into account (or in regions where  $N$  is dominated by the thermal stratification), the required work against

gravity is reduced by  $K_T/\eta$ , as in the case of hydrodynamic instabilities (§ 2.2.4 and 2.3.2). The modified instability criterion then reads

$$\frac{\omega_A}{\Omega} > \left(\frac{N}{\Omega}\right)^{1/2} \left(\frac{K_T}{r^2\Omega}\right)^{1/4} \left(\frac{\eta}{K_T}\right)^{1/2} \quad (3.24)$$

(Spruit 1999). For a sufficiently large magnetic field, there is a range of radial scales that are unstable with the largest unstable scale limited by stratification (Eq. 3.20) and the smallest scale, by magnetic diffusivity (Eq. 3.22). These small scales produce *turbulent* magnetic diffusivity given by the equality in Eqs. (3.23) and (3.24)

$$\eta_{e0} = r^2\Omega \left(\frac{\omega_A}{\Omega}\right)^4 \left(\frac{\Omega}{N}\right)^2 \quad \text{or} \quad \eta_{e1} = r^2\Omega \left(\frac{\omega_A}{\Omega}\right)^2 \left(\frac{\Omega}{N}\right)^{1/2} \left(\frac{K_T}{r^2N}\right)^{1/2} \quad (3.25)$$

in cases with (0) and without (1) thermal diffusivity.

Spruit (2002) made further assumptions to produce a model that can be used in stellar evolution codes. Equating the growth-rate of  $B_\phi$  (Eq. 3.21) with the amplification time of the Tayler-Spruit instability

$$\tau = \frac{N}{\omega_A\Omega q} \quad \text{with} \quad q = \left| \frac{\partial \ln \Omega}{\partial \ln r} \right|, \quad (3.26)$$

he obtains a relation between the Alfvén frequency (or equivalently, the amplitude of the magnetic field) and the differential rotation

$$\frac{\omega_A}{\Omega} = q \frac{\Omega}{N} \quad (3.27)$$

valid in the absence of thermal diffusivity and

$$\frac{\omega_A}{\Omega} = q^{1/2} \left(\frac{\Omega}{N}\right)^{1/8} \left(\frac{K_T}{r^2N}\right)^{1/8} \quad (3.28)$$

when  $K_T$  cannot be neglected.

Feed back to the rotation profile occurs through magnetic stresses. Still assuming  $B_\phi \gg B_r$ , one gets

$$B_\phi = (4\pi\rho)^{1/2} r\omega_A \quad \text{and} \quad B_r = \frac{l_r}{l_h} B_\phi \approx \frac{l_r}{r} B_\phi \quad (3.29)$$

( $l_r$  is obtained by assuming the equality in condition 3.20). Magnetic stresses are then of the form

$$S_0 = \frac{1}{4\pi} B_r B_\phi = \rho r^2 \Omega^2 q^3 \left(\frac{\Omega}{N}\right)^4 \quad \text{or} \quad S_1 = \rho r^2 \Omega^2 q \left(\frac{\Omega}{N}\right)^{1/2} \left(\frac{K_T}{r^2N}\right)^{1/2} \quad (3.30)$$

and this corresponds to a viscosity for the vertical transport of angular momentum

$$\nu_{\text{TS0}} = \frac{S}{\rho q \Omega} = r^2 \Omega q^2 \left(\frac{\Omega}{N}\right)^4 \quad \text{or} \quad \nu_{\text{TS1}} = r^2 \Omega \left(\frac{\Omega}{N}\right)^{1/2} \left(\frac{K_T}{r^2N}\right)^{1/2} \quad (3.31)$$

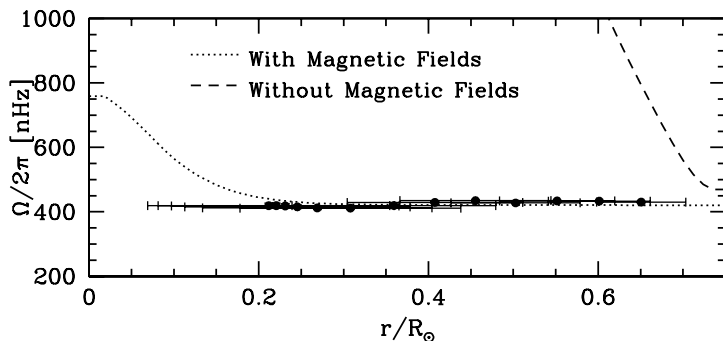


**Fig. 17.** Rotation profile at the solar age for a model with meridional circulation and shear instability (dashed line) and with also the contribution of the Tayler-Spruit instability (dotted line). The initial velocity is  $50 \text{ km s}^{-1}$ , and surface braking follows Kawaler (1988). Dots with error bars correspond to the helioseismic solar rotation (Couvrad et al. 2003). From Eggenberger et al. (2005).

with indexes (0) and (1) representing cases with and without thermal diffusivity (Spruit 2002). Maeder & Meynet (2004) made a more general formulation, which takes into account intermediate regimes.

### 3.7.1 Applications to stars

This model has been applied by the Geneva group to a variety of stellar models. This process is highly efficient in reducing differential rotation. In the case of massive stars, rotation gradients are strongly reduced by the Tayler-Spruit instability (Maeder & Meynet 2004). Shear instabilities become much less important in this case, while meridional circulation is revived, since the rotation profile remains far from the one required by thermal equilibrium (§ 2.4.2). These results are discussed at length by Meynet (2007, this volume).

In the case of the Sun, the Tayler-Spruit instability also strongly reduces differential rotation. This was tested in an evolutionary model of a  $1 M_{\odot}$  model, in which are also included meridional circulation and shear instability (Eggenberger, Maeder & Meynet 2005). This study confirms the capability of this process to reproduce the Sun’s flat rotation profile (see Fig. 17).

### 3.8 Open problems in the coupling of magnetic fields and rotation

The existence of the Tayler-Spruit instability has been observed in numerical simulations (Braithwaite 2006). However, the interaction of this instability with the star’s rotation with the mechanism described above implicitly assumes the regeneration of a large scale, axisymmetric poloidal field from which the toroidal field can be generated. However, the “kink” instability described here corresponds to a global  $m = 1$  mode, and so generates a poloidal field with a similar angular dependence, and not the axisymmetric field that is required in the model. This

was also shown in numerical simulations by Zahn, Mathis & Brun (2007). In their simulations, the dynamo for the poloidal field assumed by Spruit (2002) is not present. It remains to be seen if it would occur in conditions with smaller values of  $\eta$  and  $\nu$  as expected in stellar interiors.

Another approach to the interaction of magnetic fields and rotation consists in adding the Lorentz force in the equations for meridional circulation (Mathis & Zahn 2005). This leads to a complex set of 16 coupled differential equations that has not yet been included in actual stellar evolution calculations.

## 4 Internal gravity waves

### 4.1 Introduction

A stratified fluid is one in which the density changes with height. In the oceans, such stratifications are stable if there is a continuous decrease in density with height; that is, lighter fluid is always located above heavier fluid. In the Earth's atmosphere and in stars, one has to remove the adiabatic temperature gradient when making this comparison. This gives rise to the well known Schwarzschild criterion.

When a stable stratification is disturbed by a perturbation, buoyancy and gravity tend to restore the fluid to its previous equilibrium. For example, when a fluid parcel is displaced upward into a less dense region, gravity pulls it back down, below its equilibrium position and thus, into a denser region. Buoyancy takes over and pushes it upward. The fluid parcel “overshoots” to the less dense region and the cycle repeats. This oscillatory behavior forms what is called an internal gravity wave.

In the Earth's atmosphere, wave induced momentum transport is a key element in the understanding of several phenomena; the most famous is the quasi-biennial oscillation (or QBO), which is an alternating pattern of westerly and easterly mean zonal winds observed in the stratosphere close to the equator.

In astrophysics, internal gravity waves have initially been invoked as a source of mixing for elements induced by a variety of mechanisms (Press 1981, García López & Spruit 1991, Schatzman 1993, Montalbán 1994, Montalbán & Schatzman 1996, 2000, Young et al. 2003, see § 4.4). Ando (1986) studied the transport of momentum associated with standing gravity waves; he showed how angular momentum redistribution by these waves may increase the surface velocity to induce episodic mass-loss in Be stars (see also Lee 2006). He was the first to clearly state (in the stellar context) the fact that waves carry angular momentum from the region where they are excited to the region where they are dissipated. Goldreich & Nicholson (1989, see also Zahn 1975) later invoked gravity waves in order to explain the evolution of the velocity of binary stars, producing synchronization that proceeds from the surface to the core. Traveling internal gravity waves have since been invoked as an important process in the redistribution of angular momentum in single stars spun down by a magnetic torque (Schatzman 1993, Kumar & Quataert 1997, Zahn, Talon, & Matias 1997, Talon, Kumar, & Zahn 2002).

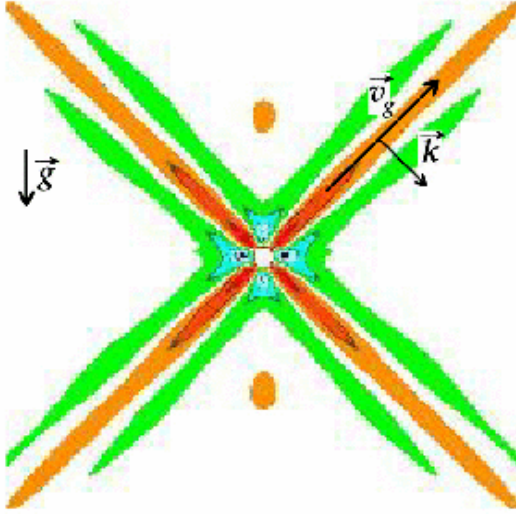


**Fig. 18.** Numerical simulation of an internal gravity wave excited by an oscillatory forced patch. Colors show density fluctuations. *Credit: Bruce R. Sutherland, U. of Alberta.*

#### 4.2 Properties of internal gravity waves

Internal gravity waves (IGWs) propagate due to buoyancy forces. Contrary to surface waves which are confined to a fluid’s interface, internal gravity waves are able to propagate both horizontally and vertically through the fluid. They exist in stratified environments and transport energy and momentum.

Because their restoring force is buoyancy, these waves are anisotropic with respect to “vertical” and “horizontal” orientations. This implies that, contrary to the case of a pressure wave, a point source does not produce an isotropic wave. Their frequency  $\sigma$  has to be lower than the Brunt-Väisälä frequency  $N$ , which is the natural oscillation frequency of a displaced element in a stratified region. We thus have

$$0 < \sigma < N \quad (4.1)$$

( $N$  is defined in § 2.2.1). In stars,  $N_T$  is typically of order  $10^{-3} \text{ s}^{-1}$ . A surprising property of internal waves is that their group velocity  $\vec{v}_g$ , which corresponds to the transport of energy is perpendicular to the phase velocity  $\vec{v}_p$  and to the wave number<sup>14</sup>  $\vec{k}$ . This is illustrated in Fig. 18.

Let us now take a more formal look at the equations which describe those waves in a differentially rotating star<sup>15</sup>. We use spherical coordinates  $(r, \theta, \phi)$ .  $\vec{e}_z$  is the unit vector along the rotation axis, and  $\vec{e}_\phi$  that in the azimuthal direction. We

<sup>14</sup>This can be demonstrated using the real part of the dispersion relation (4.22).

<sup>15</sup>Our development follows Press (1981), Goldreich & Nicholson (1989) and Zahn et al. (1997). See also Unno et al. (1989) for details regarding the derivation of the wave equation.

assume that the angular velocity  $\Omega$  depends only on depth (just as in § 2.4). In an inertial frame, the total velocity  $\vec{U}$  is

$$\vec{U}(r, \theta, \phi, t) = \Omega(r) \vec{e}_z \times \vec{r} + \vec{u}(r, \theta, \phi, t), \quad (4.2)$$

where  $\vec{u}$  is the velocity associated with the wave. The equation of motion reads

$$\frac{d\vec{u}}{dt} + \left\{ 2\Omega \vec{e}_z \times \vec{u} + \vec{e}_\phi r \sin \theta \left( \vec{u} \cdot \vec{\nabla} \Omega \right) \right\} = -\frac{1}{\rho} \vec{\nabla} P' + \frac{\rho'}{\rho} \vec{g}, \quad (4.3)$$

with

$$\frac{d}{dt} = \left( \frac{\partial}{\partial t} + \Omega \frac{\partial}{\partial \phi} \right), \quad (4.4)$$

and where  $P'$  and  $\rho'$  are the Eulerian perturbations of pressure and density respectively. We used the Cowling (1941) approximation and neglected fluctuations of the gravitational potential. Viscosity is also ignored. We also consider the continuity equation

$$\frac{d\rho'}{dt} + \vec{\nabla} \cdot \rho \vec{u} = 0, \quad (4.5)$$

and the thermodynamic relation between  $\rho'$  and  $P'$  which in the adiabatic limit reads

$$\frac{\rho'}{\rho} - \frac{1}{\Gamma_1} \frac{P'}{P} - \frac{N^2}{g} \xi_r = 0, \quad (4.6)$$

$\Gamma_1$  being the adiabatic exponent and  $\xi_r$  the radial part of the displacement and which is related to the wave velocity by  $u_r = i\sigma \xi_r$ .

We will proceed with a further simplification. Neglecting the terms in curly brackets in the equation of motion (4.3), we treat waves as if they were pure gravity waves which are not modified by the Coriolis acceleration, but just feel the entrainment by the differential rotation<sup>16</sup>. In this case, we recover the equations that describe internal waves in a non-rotating star up to replacing the derivative with respect to time by (4.4), see *e.g.* Unno et al. (1989). Solutions are then separable with respect to  $r$ ,  $\theta$ ,  $\phi$  and  $t$  and are of the form

$$u_r(r, \theta, \phi, t) = u_v(r) P_\ell^m(\cos \theta) \exp i(\sigma t - m\phi), \quad (4.7)$$

where

$$\sigma(r) = \sigma_0 - m\Omega(r), \quad (4.8)$$

with  $\sigma_0$  being the frequency in the inertial frame and  $P_\ell^m$  is the associated Legendre polynomial of order  $\ell$  and azimuthal number  $m$ . In the internal waves low

---

<sup>16</sup>The case of the gravito-inertial wave can be treated using the so-called *traditional approximation* which consists of neglecting the radial component of the Coriolis acceleration in the equation of motion. In that case, the horizontal structure can be described by Hough functions. This is discussed by Lee & Saio (1997) and Townsend (2003). The dispersion relation for gravito-inertial-Alfvén waves is discussed in Kumar, Talon, & Zahn (1999).

frequency range which is considered here, terms of order  $\sigma^2$  can be neglected; this corresponds to the anelastic approximation. The function  $\Psi(r) = \rho^{\frac{1}{2}} r^2 u_v$  then obeys the second order equation

$$\frac{d^2 \Psi}{dr^2} + \left( \frac{N^2}{\sigma^2} - 1 \right) \frac{\ell(\ell+1)}{r^2} \Psi = 0 \quad (4.9)$$

and the dispersion relation is simply

$$k^2 \sigma^2 + N^2 k_h^2 = 0 \quad (4.10)$$

(Unno et al. 1989). Here, we neglected a right hand side term of order  $H_\rho^{-2}$  which would mainly introduce phase shifts in the oscillation (*cf.* Press 1981). For future use, we introduce the vertical and horizontal wavenumbers,  $k_v$  and  $k_h$ ,

$$k_v^2 = \left( \frac{N^2}{\sigma^2} - 1 \right) \frac{\ell(\ell+1)}{r^2} = \left( \frac{N^2}{\sigma^2} - 1 \right) k_h^2. \quad (4.11)$$

This relation shows the highly anisotropic nature of internal waves, especially in the stellar context where we are mainly looking at waves with  $\sigma \ll N$ . When the wave is propagating,  $\ell$  is conserved,  $k_h$  varies as  $1/r^2$  and  $k_v$  is modified according to (4.11) when the local frequency  $\sigma$  and/or the Brunt-Väisälä frequency  $N$  change. If  $\sigma \geq N$ ,  $k_v$  becomes imaginary and the wave is reflected. When  $\sigma \ll N$ , we have  $r k_v \gg 1$  and therefore the differential equation (4.9) may be solved by the WKB method, which yields

$$u_r = C r^{-\frac{3}{2}} \rho^{-\frac{1}{2}} \left( \frac{N^2}{\sigma^2} - 1 \right)^{-\frac{1}{4}} P_\ell^m(\cos \theta) \cos \left( \sigma t - m\phi - \int_r^{r_c} k_v dr \right), \quad (4.12)$$

with  $r_c$  designating the base of the convection zone<sup>17</sup> and  $C$  is related to the wave amplitude. It describes a monochromatic wave of local frequency  $\sigma$ , which propagates<sup>18</sup> with a vertical group velocity

$$v_g = \frac{d\sigma}{dk_v} = -\frac{\sigma}{k_v} \frac{N^2 - \sigma^2}{N^2} \quad (4.13)$$

and horizontal velocities

$$u_\phi = -m \frac{r k_v}{\ell(\ell+1)} \frac{u_r}{\sin \theta} \quad (4.14)$$

and

$$u_\theta^2 + u_\phi^2 = \left( \frac{N^2}{\sigma^2} - 1 \right) u_r^2. \quad (4.15)$$

---

<sup>17</sup>Here, we are implicitly assuming that IGWs are generated in the outer convection zone and travel inwards.

<sup>18</sup>The most general solution would include a stationary wave.

The  $\phi$  component of the velocity field depends on the azimuthal number  $m$ . In a rotating star, we distinguish between *prograde* ( $m > 0$ ) and *retrograde* ( $m < 0$ ) waves, corresponding respectively to waves traveling in the direction of rotation or against it<sup>19</sup>.

So far, nonadiabatic effects have not been taken into account. To do so, we follow Press (1981) once more, and consider damping by thermal diffusion in the Boussinesq approximation<sup>20</sup> and in Cartesian coordinates<sup>21</sup>. In that case, the equation of motion reads

$$i\sigma\nabla^2(\rho u_r) = gk_h^2\rho' \quad (4.16)$$

while the equation of state may be written

$$\frac{\rho'}{\rho} = -\delta\frac{T'}{T} + \varphi\frac{\mu'}{\mu}, \quad (4.17)$$

where we again ignored the pressure perturbation. The fluctuation of  $\mu$  is given by the conservation of mean molecular weight in the wave motion

$$i\sigma\frac{\mu'}{\mu} = \frac{\nabla_\mu}{H_P} u_r, \quad (4.18)$$

and that of  $T$  by the heat equation

$$i\sigma\frac{T'}{T} = -(\nabla_{\text{ad}} - \nabla)\frac{u_r}{H_P} + \frac{K}{T}\nabla^2 T', \quad (4.19)$$

where  $K$  is the thermal diffusivity. Combining Eqs. (4.17), (4.18) and (4.19), we obtain

$$(i\sigma - K\nabla^2)\rho' = \frac{N^2}{g}\rho u_r - \frac{K}{i\sigma}\nabla^2\left(\frac{N_\mu^2}{g}\rho u_r\right), \quad (4.20)$$

and with (4.16), we get the wave equation

$$\left(\nabla^2 + k_h^2\frac{N^2}{\sigma^2}\right)\rho u_r + i\frac{K}{\sigma}\nabla^2\left(\nabla^2 + k_h^2\frac{N_\mu^2}{\sigma^2}\right)\rho u_r = 0. \quad (4.21)$$

From this equation, we derive the dispersion relation

$$\left[k_v^2 - k_h^2\left(\frac{N^2}{\sigma^2} - 1\right)\right] - i\frac{K}{\sigma}\left[k_v^2 + k_h^2\right]\left[k_v^2 - k_h^2\left(\frac{N_\mu^2}{\sigma^2} - 1\right)\right] = 0. \quad (4.22)$$

We now have Eq. (4.9) which is the adiabatic equation in spherical geometry while Eq. (4.21) takes into account non-adiabaticity. We combine wanted features

<sup>19</sup>Note that some authors, including Unno et al. (1989), define the wave velocity as  $u_r \propto \exp(im\phi)$  instead of  $u_r \propto \exp(-im\phi)$  as used here.

<sup>20</sup>Here, the continuity equation (4.5) is replaced by  $\vec{\nabla} \cdot \vec{u} = 0$ , and implies that vertical variations of density are not considered in that equation.

<sup>21</sup>This derivation with mean molecular weight gradients is taken from Zahn et al. (1997).

from both these equations to obtain an equation that is locally Boussinesq and globally anelastic, and that takes into account nonadiabatic effects

$$\frac{d^2\Psi}{dr^2} + \left(\frac{N^2}{\sigma^2} - 1\right) \frac{\ell(\ell+1)}{r^2} \Psi + i \frac{K}{\sigma} \nabla^2 \left( \nabla^2 + k_h^2 \frac{N^2}{\sigma^2} \right) \Psi = 0. \quad (4.23)$$

As long as thermal damping is not too large<sup>22</sup>, the WKB solution for this equation is still given by equation (4.12), but multiplied by a damping factor  $\exp(-\tau/2)$  where

$$\tau(r, \sigma, \ell) = [\ell(\ell+1)]^{\frac{3}{2}} \int_r^{r_c} K \frac{N N_T^2}{\sigma^4} \left( \frac{N^2}{N^2 - \sigma^2} \right)^{\frac{1}{2}} \frac{dr}{r^3}. \quad (4.24)$$

### 4.3 Excitation of internal waves

In the Earth's atmosphere, IGWs are generated by several processes, like *e.g.* convection and wind compression by topography. In the single star context, we are interested by waves produced by the injection of kinetic energy from a turbulent region to an adjacent stable region<sup>23</sup>. In the Earth's atmosphere, this is observed at the border of clouds (Townsend 1965). The existence of those waves in stars is observed in numerical simulations of penetrative convection both in 2-D and 3-D (Hurlburt et al. 1986, 1994, Andersen 1994, Nordlund et al. 1996, Kiraga et al. 2000, Dintrans et al. 2005, Rogers & Glatzmeier 2005a,b). They are excited by two different processes namely

- convective overshooting in a stable region;
- excitation by the Reynolds stresses in the convection zone itself.

Both sources contribute to the excitation.

Ultimately, one would like to obtain realistic wave fluxes from numerical simulation themselves. Some improvement for such prescriptions has been made by Rogers & Glatzmeier (2005b) who calculated wave excitation in a cylindrical (2-D) model having a stratification that is similar to that of the Sun. However, the level of turbulence reached in that simulation is far from realistic and thus, cannot provide a good answer to the question yet. Furthermore, an analysis of the wave spectrum characteristics as a function of convective properties (such as the convective luminosity and/or the turn-over time-scale) has not been done. For stellar applications, the variation of wave generation with effective temperature<sup>24</sup> is a key feature in understanding their differential properties (see §4.6.2). These are the two reasons why we will rather rely on theoretical estimates for wave generation.

---

<sup>22</sup>If the imaginary part of this equation is larger than the real part, the solution for  $u_r$  is evanescent rather than oscillatory.

<sup>23</sup>In binary stars, the variation of the gravitational potential can excite a gravity wave in early type stars. Its effect has been studied by Zahn (1975a) and Goldreich & Nicholson (1989).

<sup>24</sup>One should note that the properties of the surface convection zone, like its depth and relevant time-scales, are determined almost uniquely by the star's surface temperature.

Excitation by overshooting is quite difficult to evaluate analytically. García López & Spruit (1991) made such an attempt and assumed that the pressure perturbation produced by turbulent eddies at the radiative/convective boundary is equal to the wave pressure perturbation. In this model, small stochastic eddies combine to excite a whole wavelength spectrum. It has been formulated under the assumption of homogeneous turbulence, but it could be modified to incorporate the presence of down-drafts as observed in numerical simulations. Comparisons of numerical results with this theoretical model show that the maximum in the wave spectrum produced by the simulation was similar in amplitude to that of this parametric model (Kiraga et al. 2003, Rogers & Glatzmeier 2005b). However, in simulations, modes were excited over a much broader range of frequencies and wavelengths. It is not clear whether this is related to the bi-dimensional nature of the simulations or to shortcomings in the model.

Another estimate for excitation by overshooting has been made by Fritts, Vadas, & Andreassen (1998), in a study aimed at estimating the residual circulation induced by latitude dependent wave dissipation in the tachocline. However, they concentrate on the small wavelength waves that dissipate close to the convection zone, and their mechanism does not take the combination of small scale eddies into account in order to produce low degree waves. Such waves are essential in order to influence the inner regions on an evolutionary time-scale (§ 4.5, see also Talon, Kumar, & Zahn 2002). Let us also note that such low degree waves are actually observed in the wave spectra of numerical simulations.

IGWs can also be excited in the convection zone itself. That can be estimated by convolving the local wave function, which is evanescent and whose local amplitude is proportional to  $\exp[-\int dr k_r]$ , with entropy fluctuations and Reynolds stresses. A complete description of this process has been developed by Goldreich and his collaborators (Goldreich & Keeley 1977, Goldreich & Kumar 1990, Goldreich, Murray, & Kumar 1994, hereafter GMK). Their model was first applied to the solar p-modes, and quite successfully reproduces the solar spectral energy input rate distribution, provided one free parameter which describes the geometry of turbulent eddies is calibrated. In that case, driving is dominated by entropy fluctuations. Balmforth (1992) made a similar study, using a somewhat different formalism. Subject to the calibration of a free parameter, he is also able to reproduce the spectral energy distribution; however, Reynolds-stresses dominate the driving in his calculations.

The GMK formalism can be adapted to the case of g-modes (Kumar & Quataert 1997); the energy flux per unit frequency  $\mathcal{F}_E$  is then

$$\begin{aligned} \mathcal{F}_E(\ell, \sigma) &= \frac{\sigma^2}{4\pi} \int dr \frac{\rho^2}{r^2} \left[ \left( \frac{\partial \xi_r}{\partial r} \right)^2 + \ell(\ell+1) \left( \frac{\partial \xi_h}{\partial r} \right)^2 \right] \\ &\times \exp \left[ -h_\sigma^2 \frac{\ell(\ell+1)}{2r^2} \right] \frac{v^3 L^4}{1 + (\sigma\tau_L)^{\frac{15}{2}}}, \end{aligned} \quad (4.25)$$

where  $\xi_r$  and  $[\ell(\ell+1)]^{\frac{1}{2}} \xi_h$  are the radial and horizontal displacement wave-functions, which are normalized to unit energy flux just below the convection zone,  $v$  is the

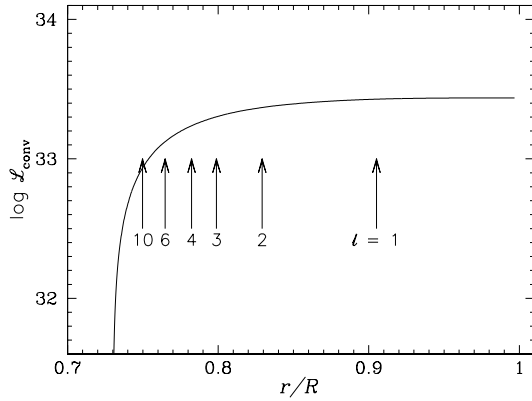


**Fig. 19.** Penetration of IGW into the convection zone of a ZAMS  $1 M_{\odot}$  model for various degrees  $\ell$ . The arrows indicate the depth where the amplitude is reduced by a factor of 2. Also shown is the local convective flux given by the mixing length theory.

convective velocity,  $L$  the radial size of an energy bearing turbulent eddy,  $\tau_L \approx L/v$  the characteristic convective time, and  $h_{\sigma}$  is the radial size of the largest eddy at depth  $r$  with characteristic frequency of  $\sigma$  or greater ( $h_{\sigma} = L \min\{1, (2\sigma\tau_L)^{-\frac{3}{2}}\}$ ).

In the convection zone, the mode is evanescent and the penetration depth<sup>25</sup> is inversely proportional to  $\sqrt{\ell(\ell+1)}$ . Figure 19 compares this distance for various modes with the convective energy that is locally available. In the outer part of the model, the luminosity is carried almost uniquely by convection.

#### 4.4 Particle transport

While we all learned in basic physics lectures that waves do not produce transport of matter, this is actually only true when a first order, linear approximation is used. In fact, there exists a wide range of physical processes that may give rise to mixing by waves, and we will briefly review some of these here. Let us note however that the actual calculations that were made with these in a stellar context do not take into account angular momentum transport by the same waves, which would greatly reduce their penetration depth (see § 4.5) and thus, the (numerical) results that are mentioned should be reviewed accordingly.

##### 4.4.1 Shear unstable waves

Let us look at the case of low frequency IGWs in which  $\sigma \ll N$ . Then, the velocity of the associated flow is nearly horizontal, and produces a sinusoidally varying vertical shear. Such a flow has inflection points, which may trigger a shear

<sup>25</sup>This is the theoretical dependence. Damping can be enhanced by turbulence, which would reduce the surface amplitude of the mode (see *e.g.* Andersen 1996).

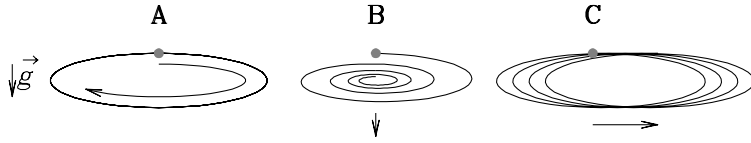


**Fig. 20.** Movement of a fluid parcel (whose initial position is shown with a gray dot) when a wave passes in the linear regime (**A**), when thermal diffusion is taken into account (**B**) and when non-linearities are taken into account (**C**). In (**B**), the net displacement is in the direction of gravity while in (**C**), it is perpendicular to  $\vec{g}$ .

instability that will produce small scale turbulence. Because the flow is time-dependent, the shear rate  $k_v u_h$  has to be larger than the wave frequency for this to occur and hence the condition for weak mixing by this process is (Press 1981, García López & Spruit 1991)

$$k_v u_h > \sigma. \quad (4.26)$$

When this condition is satisfied, the local shear rate can be compared to the stabilizing Brunt-Väisälä frequency, leading to the well known Richardson criterion. Instability occurs when

$$Ri = \frac{N^2}{(k_v u_h)^2} < \frac{1}{4}. \quad (4.27)$$

Taking thermal diffusivity into account, the Richardson criterion is modified and becomes

$$\frac{N^2}{(k_v u_h)^2} \frac{\ell_0 v_0}{K} < \frac{1}{4} \quad (4.28)$$

where  $\ell_0 v_0 = D_0$  is the turbulent diffusion associated with eddies of size  $\ell_0$  and velocity  $v_0$ . The actual turbulent diffusion  $D_{\text{wave shear}}$  will be given by the largest value of this product that is unstable and thus

$$D_{\text{wave shear}} = \frac{1}{4} \frac{(k_v u_h)^2}{N^2} K. \quad (4.29)$$

García López & Spruit (1991) applied such a formula to the case of F stars, in order to reproduce the so-called Li dip (see § 4.6.2). Using an excitation model based on the matching of pressure fluctuations at the base of the convection zone and that of the waves, they showed that Li burning could be produced in the dip region if the input of turbulent energy in waves is large enough<sup>26</sup> and provided the mixing length of convection is suitably chosen.

<sup>26</sup>In their paper, García López & Spruit multiplied the wave flux calculated using a standard mixing length approach of convection by 10 to obtain enough depletion in the Li-dip. This could be explained by considering the presence of plumes in convection.

#### 4.4.2 Irreversible second-order stochastic diffusion

In the adiabatic and linear limit, the trajectory of a fluid parcel as a wave passes is a simple circular movement (Fig. 20A). However, when thermal diffusion is taken into account, the “memory” of the initial entropy content is lost, and the fluid parcel does not return to its initial entropy level (Fig. 20B; Press 1981, Schatzman 1993, Montalbán 1994). In the adiabatic limit, the vertical displacement of the fluid element is given by  $\delta_v = u_v/\sigma$ , while in the absence of a restoring force it would be  $\Delta_v = k_v \delta_v^2$ . The fraction of entropy that is lost during a vertical excursion can be roughly estimated as the fraction of this length-scale  $\Delta_v$  corresponding to the ratio of the diffusive time-scale  $K k_v^2$  and the period  $1/\sigma$ . Overall, the vertical displacement of the fluid parcel is

$$\ell = K \frac{k_v^3 u_v^2}{\sigma^3} \quad (4.30)$$

(Press 1981). The velocity scale associated with this process is

$$v = \ell \sigma, \quad (4.31)$$

and this leads to a diffusion coefficient of the form

$$D_{2\text{nd order}} \equiv \ell v = K^2 \frac{k_v^6 u_v^4}{\sigma^5} \quad (4.32)$$

for one wave. A combination of all excited waves has to be made to transform this into a global diffusion coefficient (this is discussed at length by Montalbán 1994). This process should be efficient only over about one damping length scale and thus, will lead to a diffusion coefficient that decreases quite rapidly with depth. Calculations using such a description were made by Montalbán & Schatzman (1996) to compute Li destruction in cool main sequence stars.

#### 4.4.3 Stokes’ drift

*Stokes’ drift* can be defined as the difference between the mean fluid velocity measured at a point and the mean velocity of a drifter in the direction of wave propagation and was originally described by Stokes (1847, see Lighthill 1979 for a complete description). If there is no mean velocity, it represents the velocity of a passive scalar that is slowly moving through the fluid. This displacement is in the direction of wave propagation ( $\vec{v}_p$ ), which is mainly horizontal for the IGWs we are studying here. Heuristically, this drift is caused by an asymmetry between the horizontal displacement when the wave is moving downward and upward. The resulting movement is shown in Fig. 20C. In the case of stars, this will produce mainly a horizontal redistribution of elements and thus, little vertical mixing is expected from this process.

#### 4.4.4 Wave-induced turbulence

The last process I will describe here is wave-induced turbulence. This has been discussed by a few authors, under various forms. Canuto (2002) developed a model in which gravity waves act as a source term in the equation that describes turbulence. Young et al. (2003) describe mixing by waves generated at the boundary of a convective region as a physical description of “overshooting”. Talon & Charbonnel (2005) study the formation of an oscillating shear layer caused by differential wave damping (see §4.5.1). In that process, energy is transferred by waves from the convection zone to the shear layer and stored in differential rotation, which can then be converted to turbulence by the shear instability (§2.3.2). Let us note that it is different from the process described in §4.4.1: here it is the rotation profile that becomes unstable, and not the wave itself.

In all these cases, turbulent mixing should be large in a rather small region just below the convection zone, and acts to smooth out the possible chemical discontinuity at convective boundaries.

#### 4.5 Momentum transport

Let us now describe how angular momentum is transported by IGWs<sup>27</sup>. First, the horizontal average of the kinetic energy density can be calculated from the WKB velocities (4.12) and (4.15) and yield

$$\begin{aligned} \frac{1}{2} \rho \langle u^2 \rangle &\equiv \frac{1}{4\pi} \iint \frac{1}{2} \rho (u_r^2 + u_\theta^2 + u_\phi^2) \sin \theta \, d\theta \, d\phi \\ &= \frac{1}{2} \frac{N^2}{\sigma^2} \frac{1}{4\pi} \iint \rho u_r^2 \sin \theta \, d\theta \, d\phi \equiv \frac{1}{2} \frac{N^2}{\sigma^2} \rho \langle u_r^2 \rangle. \end{aligned} \quad (4.33)$$

We now multiply this quantity by the group velocity (4.13) to get the average kinetic energy flux carried by a traveling IGW

$$\mathcal{F}_{K,\sigma,\ell,m} = -\frac{1}{2} \rho \langle u^2 \rangle \frac{\sigma}{k_v} \frac{N^2 - \sigma^2}{N^2} = -\frac{1}{2} \rho \langle u^2 \rangle \frac{\sigma^2}{N^2} \frac{(N^2 - \sigma^2)^{\frac{1}{2}}}{k_h}. \quad (4.34)$$

The mean radial flux of angular momentum is evaluated using Eqs. (4.12), (4.14), (4.33) and (4.34)

$$\begin{aligned} \mathcal{F}_{J,\sigma,\ell,m} &= \frac{1}{4\pi} \iint \rho r \sin \theta u_\phi u_r \sin \theta \, d\theta \, d\phi \\ &= -m r \frac{r k_v}{\ell(\ell+1)} \frac{1}{4\pi} \iint \rho u_r^2 \sin \theta \, d\theta \, d\phi = 2 \frac{m}{\sigma} \mathcal{F}_{K,\sigma,\ell,m}. \end{aligned} \quad (4.35)$$

Inserting (4.12) into (4.35), it is possible to verify that, in the adiabatic limit, the

---

<sup>27</sup>This description follows Zahn et al. (1997).

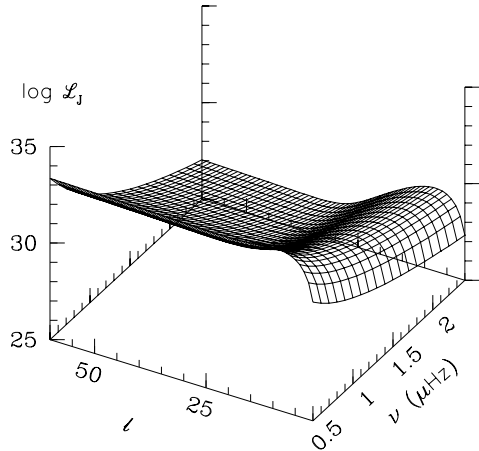


**Fig. 21.** Angular momentum wave luminosity  $\mathcal{L}_{J,\sigma,\ell}$  in a ZAMS  $1 M_{\odot}$  model for various degrees  $\ell$  and frequencies  $\nu = \sigma/2\pi$  according to the GMK model.

angular momentum luminosity is conserved<sup>28</sup>

$$4\pi r^2 \mathcal{F}_{J,\sigma,\ell,m}(r) \equiv \mathcal{L}_{J,\sigma,\ell,m} = \text{cst.} \quad (4.36)$$

Figure 21 shows the wave spectrum of angular momentum luminosity in a  $1 M_{\odot}$  model when the GMK model is used for the kinetic energy flux.

When radiative damping is taken into account, the wave amplitude is multiplied by an attenuation factor  $\exp(-\tau/2)$  (*cf.* Eq. 4.24). Locally, the total angular momentum luminosity is the sum of the contribution of all waves

$$\mathcal{L}_J(r) = \sum_{\text{waves}} \mathcal{L}_{J,\sigma,\ell,m}(r_c) \exp[-\tau(r, \sigma, \ell)]. \quad (4.37)$$

The deposition of angular momentum is then given by the radial derivative of this luminosity. Let us remark that here we consider only the radial dependency of wave transport, thus the use of horizontal averaging. When other processes for angular momentum redistribution are also taken into account, the evolution of angular momentum follows

$$\rho \frac{d}{dt} [r^2 \Omega] = \frac{1}{5r^2} \frac{\partial}{\partial r} [\rho r^4 \Omega U] + \frac{1}{r^2} \frac{\partial}{\partial r} \left[ \rho \nu_t r^4 \frac{\partial \Omega}{\partial r} \right] \pm \frac{3}{8\pi} \frac{1}{r^2} \frac{\partial}{\partial r} \mathcal{L}_J(r), \quad (4.38)$$

where  $U$  is the radial meridional circulation velocity and  $\nu_t$  the viscosity from hydrodynamical instabilities (§ 2.2)<sup>29</sup>. The “+” (“−”) sign in front of the angular momentum luminosity corresponds to a wave traveling inward (outward).

<sup>28</sup>On the other hand, the kinetic energy of the wave varies with depth since the local frequency  $\sigma$  depends on the rotation rate  $\Omega(r)$ . Bretherton (1969) showed that, in the plane-parallel case, conservation is ensured in the inertial frame.

<sup>29</sup>One could also add the magnetic viscosity of § 3.7, but for consistency gravito-Alfvén waves should then be considered. See *e.g.* Barnes, MacGregor & Charbonneau 1998.

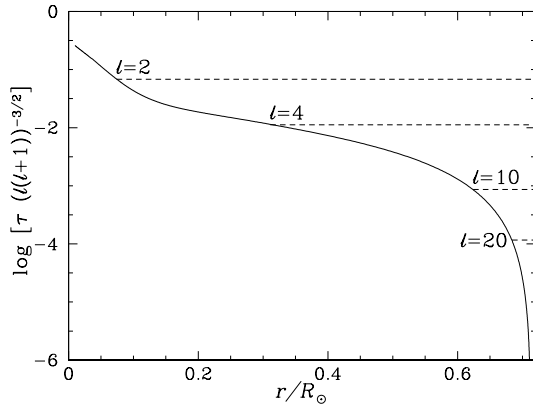


**Fig. 22.** Evaluation of the damping factor  $\tau$  (cf. Eq.4.24) for a frequency of  $1 \mu\text{Hz}$  in a solar model. The depth corresponding to an attenuation by a factor  $1/e$  is shown for various degrees  $\ell$ .

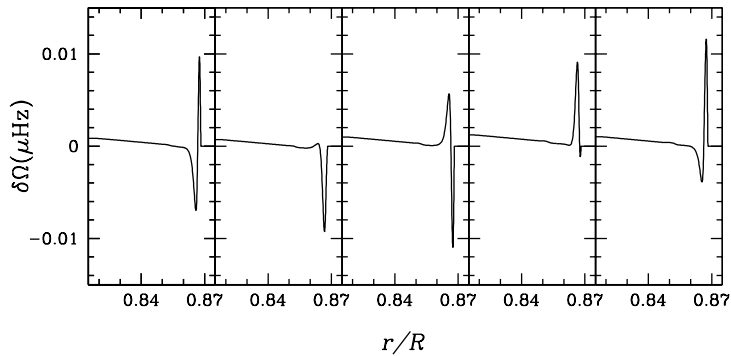


**Fig. 23.** Shear layer oscillation (SLO) in a  $1.3 M_{\odot}$  model. Successive profiles are separated by 1 year intervals. The layer's thickness depends on the magnitude of thermal dissipation and the oscillation period is a function of the total wave angular momentum luminosity.

#### 4.5.1 Wave-mean flow interaction and the SLO

We now examine the impact of IGWs on the radial distribution of angular momentum. Figure 22 shows the penetration depth for waves of various degrees. For low frequency waves, damping is strong enough so that most waves are damped very close to the base of the convection zone. These are the waves we will examine here.

Let us first take a look at the damping integral (4.24), and assume that both prograde and retrograde waves are excited with the same amplitude (according to Eq. 4.25). In solid body rotation, both waves are equally dissipated when traveling inward and there is no impact on the distribution of angular momentum. In the

presence of differential rotation, the situation is different. If the interior is rotating faster than the convection zone, the local frequency of prograde waves diminishes, which enhances their dissipation; the corresponding retrograde waves are then dissipated further inside. This produces an increase of the local differential rotation, and creates a double-peaked shear layer<sup>30</sup>. In the presence of shear turbulence, this layer oscillates, producing a “shear layer oscillation” or SLO (*cf.* Fig. 23 and Gough & McIntyre 1998, Ringot 1998, Kumar, Talon, & Zahn 1999). Viscosity is essential in this process and is responsible for the disappearance of the outermost peak as its slope gets steeper and the peak is slowly absorbed by the convection zone. This oscillation is similar to the Earth’s QBO (see *e.g.* McIntyre 2003 for details regarding the QBO).

#### 4.5.2 Secular effects

The SLO, by locally Doppler shifting to lower frequencies both prograde and retrograde waves, acts as an efficient IGW filter (see Eq. 4.24) and for some time there was doubt that any wave power would remain beyond (Gough & McIntyre 1998). However, Talon, Kumar, & Zahn (2002) and Talon & Charbonnel (2005) performed complete calculations of wave dissipation in the presence of a SLO and showed that the low-degree waves do conserve a significant amplitude beyond the shear layer.

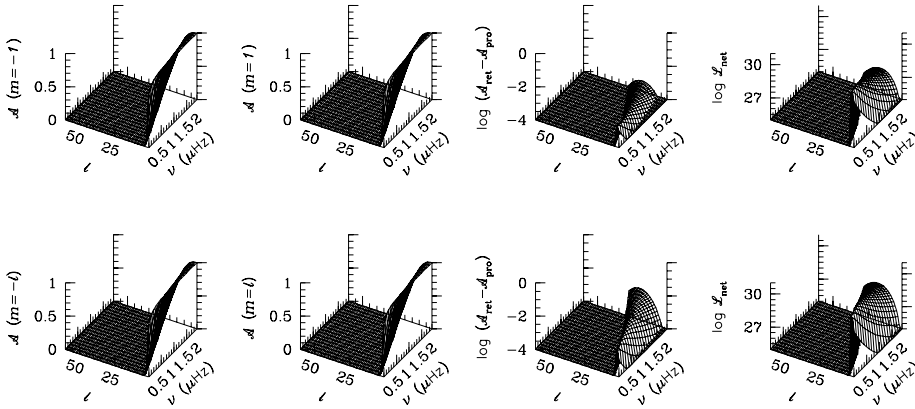
If the radiative zone has the same rotation rate as the convection zone, over a complete SLO cycle, the magnitude of the prograde and retrograde peaks<sup>31</sup> are on average equal, and waves of azimuthal number  $+m$  and  $-m$  have (on average) equal amplitudes after crossing the SLO. In the presence of differential rotation however, with the inner part rotating faster than the outer part as is the case of a solar type star that is spun down by magnetic torque, the prograde peak is always larger than the retrograde peak and there is a net flux of negative angular momentum to be redistributed in the star’s radiative zone. Talon, Kumar, & Zahn (2002) showed that this can spin down the interior of a star over long time-scales. Talon & Charbonnel (2005) later showed that this *asymmetric filtering* depends only on the difference of rotation rates at the base of the convection zone and at the base of the SLO ( $\delta\Omega = \Omega_{cz} - \Omega_{SLO}$ ).

Figure 24 shows how wave amplitudes are differentially reduced by crossing the shear layer. The rightmost column shows the net luminosity beyond the SLO; the low-frequency, low-degree waves have the strongest impact on the secular redistribution of angular momentum in the radiative part of the star. They must be low-frequency, otherwise differential damping is too weak, and low-degree, otherwise they are damped in the SLO rather than beyond.

---

<sup>30</sup>Because local shears are amplified by waves, even a small perturbation will trigger this.

<sup>31</sup>The prograde peak refers to the layer that is rotating more rapidly than the convection zone and it produces filtering of prograde waves, while the retrograde peak is rotating slower and filters retrograde waves.



**Fig. 24.** Wave characteristics below the shear layer for a differential rotation of  $\delta\Omega = 0.1 \mu\text{Hz}$  over 5% in radius in a  $1.3 M_{\odot}$  star. *First and second columns:* Wave amplitude for  $m = \pm 1$  (*top*) and  $m = \pm l$  (*bottom*). *Third column:* Amplitude difference between retrograde and prograde waves of the same azimuthal number. *Fourth column:* Net luminosity for a given azimuthal number.

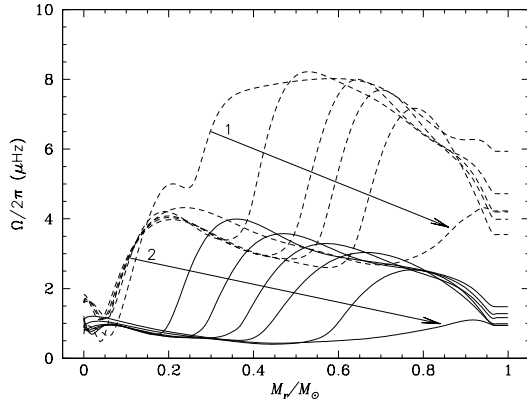


**Fig. 25.** Evolution of the interior rotation profile in a  $1 M_{\odot}$  model with meridional circulation, shear instabilities and IGWs. The initial equatorial rotation velocity is  $50 \text{ km s}^{-1}$  and surface magnetic braking is applied. Curves correspond to ages of 0.2, 0.21, 0.22, 0.23, 0.25, 0.27 (dashed lines), 0.5, 0.7, 1.0, 1.5, 3.0 and 4.6 (solid lines) Gyr. *Adapted from Charbonnel & Talon (2005).*

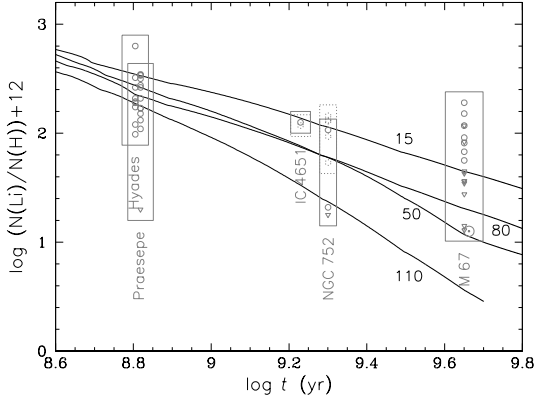


**Fig. 26.** Evolution of the surface lithium abundance for various initial rotation velocities in models including meridional circulation, shear instabilities and IGWs. The surface Li abundances as measured in various clusters are also shown. The vertical extent of boxes shows the range of lithium values for stars with an effective temperature corresponding to that of the model  $\pm 100$  K at the cluster age plus a typical error in abundance determination. *Adapted from Charbonnel & Talon (2005).*

## 4.6 Applications of angular momentum transport

### 4.6.1 The solar rotation

This description of IGWs has been applied to the solar rotation problem. Talon, Kumar, & Zahn (2002) proved, in a static solar model, that IGWs could be responsible for the required angular momentum extraction. More recently, Charbonnel & Talon (2005) revisited the problem and looked at the role of IGWs in an evolving solar model, which undergoes spin-down from the zero age main sequence (ZAMS) on. They showed that, at the age of the Sun, differential rotation indeed becomes quite small (see Fig. 25). In this simulation, the low-degree waves penetrate all the way to the core and spin it down extremely efficiently at the very beginning of the evolution. This is due to the small amount of angular momentum ( $\propto r^2$ ) contained in the core. Once the core has been spun down, the damping of retrograde waves, that carry the negative angular momentum, increases locally. Consequently a “slowness” front forms and propagates in a wave-like way from the core to the surface. As further braking takes place, a second front forms and propagates outward. The differential wave filtering adjusts itself so as to compensate for the flux of angular momentum that is lost through the stellar wind. This explains why front propagation is fast at the beginning and then slows down, just as the spin-down rate does.

Figure 26 shows the evolution of the surface Li abundance in a solar model for various initial velocities. One should note here the (small) dispersion that is obtained when very different initial velocities are considered. This would not be the case if only meridional circulation and shear turbulence were considered since

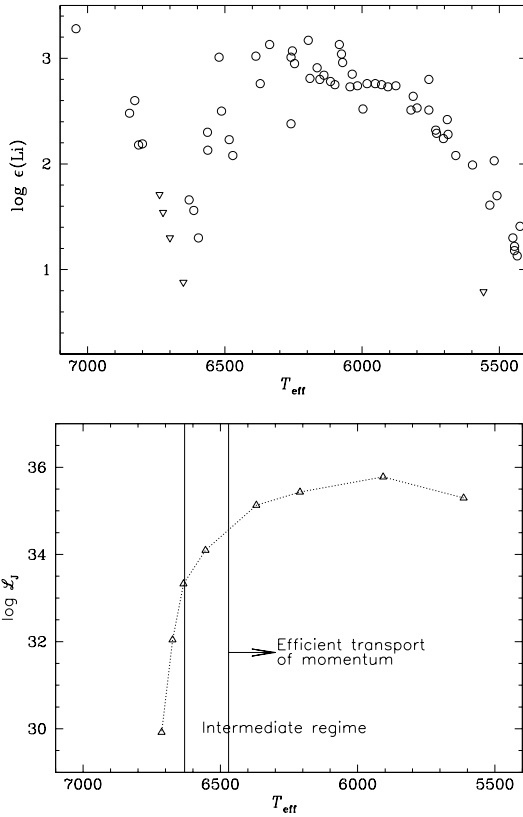


**Fig. 27.** (*top*) Lithium dip as observed in the Hyades. (*bottom*) Net angular momentum wave luminosity below the SLO for a differential rotation  $\delta\Omega = 0.05 \mu\text{Hz}$  over  $0.05 R_*$ . The vertical lines correspond to the requirements in the efficiency of angular momentum transport by a “non-standard” process so that rotational mixing would cause the Li dip as suggested by Talon & Charbonnel (1998). *Adapted from Talon & Charbonnel 2003.*

then, mixing would be proportional to the angular momentum loss.

#### 4.6.2 The Li dip

We mentioned (§ 2.5) that rotational mixing could explain the hot side of the Li dip but destroy too much lithium when looking at cooler stars. TC98 suggested that if the process that is required to explain the Sun’s rotation profile starts to become efficient in the center of the Li dip, these observations would be reconciled with rotational mixing, thus giving a model that is valid for *all* main sequence stars. One then identifies three regimes:

- Stars with  $T_{\text{eff}} \gtrsim 6900$  K have a very shallow convective envelope which is not an efficient site for magnetic generation via a dynamo process. They are

thus not slowed down by a magnetic torque. As a result, these stars soon reach the equilibrium meridional circulation (§ 2.4.2) and the associated weak mixing is just sufficient to counteract atomic diffusion.

- In stars with  $\sim 6900 \gtrsim T_{\text{eff}} \gtrsim 6600$  K, the convective envelope deepens and a weak magnetic torque appears that slows down the outer layers. In this case the transport of angular momentum by meridional circulation and shear turbulence increases, leading to a larger destruction of Li.
- Stars on the cool side of the Li dip ( $T_{\text{eff}} \lesssim 6600$  K) have an even deeper convective envelope sustaining a very efficient dynamo which produces a strong magnetic torque that spins down the outer layers very efficiently. This outer convection zone is an efficient source for IGW generation and wave-induced transport reduces the efficiency of rotational mixing, thus producing a rise in Li abundances on the cold side of the Li dip.

Talon & Charbonnel (2003) showed that the net angular momentum luminosity corresponding to IGWs does have the proper temperature dependency (Fig. 27) and thus could well explain the cool side of the lithium dip. Complete evolutionary calculations are underway to verify this proposition.

#### 4.7 Open problems in internal waves physics

While results obtained including internal waves in evolutionary models are quite promising, they remain crude, and several points are yet to be addressed. First of all, one should revisit the excitation of IGWs. Recent progress has been made in the description of the excitation of solar p-modes by considering better models for convection (see *e.g.* Belkacem et al. 2006). Work is underway to adapt this description to IGWs (Belkacem et al. in prep.) Another important point is the inclusion of the Coriolis force in calculations. This issue has been raised by several authors (Talon 1997, Lee & Saio 1997, Townsend 2003 and Mathis 2005) and work is underway to correctly incorporate it in descriptions of momentum transport in massive stars (Pantillon, Talon & Charbonnel in prep.) Finally, all calculations that are presented here correspond to horizontal averages. Implicitly, this assumes that horizontal transport is efficient in the redistribution of angular momentum along isobars. This faces the “Rossby scale problem” already mentioned in § 2.6.

### Acknowledgments

I would like to thank Jacques Richer for his assistance in preparing the discussion on atomic diffusion and for his careful reading of this manuscript which lead to major improvements.

### References

- Acheson D.J., 1978, Phil. Trans. Roy. Soc. Lond. A289, 459  
 Alfvén H., 1942, Nature 150, 405

- Aller L.H., Chapman S., 1960, ApJ 132, 461
- Andersen B.N., 1994, Solar Phys. 152, 241
- Andersen B.N., 1996, A&A 312, 610
- Ando H., 1986, A&A 163, 97
- Balmforth N.J., 1992, MNRAS 255, 639
- Barnes G., Charbonneau P., MacGregor K.B., 1999, ApJ 511, 466
- Barnes G., MacGregor K.B., Charbonneau P., 1998, ApJ 498, L169
- Belkacem K., Samadi R., Goupil M.J., Kupka F., Baudin F., 2006, A&A 460, 183
- Boesgaard A.M., Tripicco M.J., 1986, ApJ 303, 624
- Braithwaite J., Spruit H.C., 2004, Nature 431, 819
- Braithwaite J., 2006, A&A 449, 451
- Bretherton F.P., 1969, Quart. J. R. Met. Soc. 95, 213
- Brun A.S., Zahn J.-P., 2006, A&A 457, 665
- Burgers J.M., 1969, Flow equations for composite gases, Academic Press, New York
- Canuto V.M., 1998, ApJ 505, L47
- Canuto V.M., 2002, MNRAS 337, 713
- Chaboyer B., Demarque P., Pinsonneault M.H., 1995, ApJ 441, 865
- Chaboyer B., Zahn J.-P. 1992, A&A 253, 173
- Chandrasekhar S., 1961, Hydrodynamic and Hydromagnetic Stability, Oxford University Press
- Chaplin W.J., Christensen-Dalsgaard J., Elsworth Y., Howe R., Isaak G.R., Larsen R.M., New R., Schou J., Thompson M.J., Tomczyk S., 1999, MNRAS 308, 405
- Chapman S., Cowling T.G., 1970, The Mathematical Theory of Non-Uniform Gases, Cambridge University Press, 3rd ed
- Charbonneau P. 1992, A&A 259, 134
- Charbonneau P., MacGregor K.B., 1993, ApJ 417, 762
- Charbonnel C., Talon S., 2005, Science 309, 2189
- Christensen-Dalsgaard J., Proffitt C.R., Thompson M.J., 1993, ApJ 403, 75
- Couvidat S., García R.A., Turck-Chièze S., Corbard T., Henney C.J., Jiménez-Reyes S., 2003, ApJ 597, L77
- Cowling T.G., 1941, MNRAS 101, 367
- Cowling T.G., 1951, ApJ 114, 272
- Dintrans B., Brandenburg A., Nordlund Å, Stein R.F., 2005, A&A 438, 365
- Eddington A.S., 1925, Obs. 48, 73
- Eddington A.S., 1930, in "The internal constitution of the stars"
- Eggenberger P., Maeder A., Meynet G., 2005, A&A 440, L9
- Endal A.S., Sofia S., 1976, ApJ 210, 184
- Endal A.S., Sofia S., 1978, ApJ 220, 279
- Ferraro V.C.A., 1937, MNRAS, 97, 458
- Fricke K.J., 1968, Z. Astrophys., 68, 317
- Fritts D.C., Vadas S.L., Andreassen Ø., 1998, A&A 333, 343
- Garaud P., 2002, MNRAS, 335, 707

- García López R.J., Spruit H.C., 1991, ApJ 377, 268  
Goldreich P., Keeley D.A., 1977, ApJ 212, 243  
Goldreich P., Kumar P., 1990, ApJ 363, 694  
Goldreich P., Murray N., Kumar, P., 1994, ApJ 424, 466  
Goldreich P., Nicholson P.D., 1989, ApJ 342, 1079  
Goldreich P., Schubert G., 1967, ApJ 150, 571  
Gough D. O., McIntyre M.E., 1998, Nature 394, 755  
Gratton L. 1945, Mem. Soc. Astron. Ital. 17, 5  
Høiland E., 1941, Avhandlinger Norske Videnskaps-Akademi i Oslo, I, Math.-Naturv. Klasse 11, 1  
Hurlburt N.E., Toomre J., Massaguer J.M., 1986, ApJ 311, 563  
Hurlburt N.E., Toomre J., Massaguer J.M., Zahn J.-P., 1994, ApJ 421, 245  
Kawaler S., 1988, ApJ 333, 236  
Kiraga M., Różycka M., Stepień K., Jahn K., Muthsam H., 2000, Acta Astronomica, 50, 93  
Kiraga M., Jahn K., Stepień K., Zahn J.-P., 2003, Acta Astronomica, 53, 321  
Knobloch E., Spruit H.C. 1982, A&A 113, 261  
Knobloch E., Spruit H.C. 1983, A&A 125, 59  
Kumar P., Quataert E.J., 1997, ApJ 475, L143  
Kumar P., Talon S., Zahn J.-P., 1999, ApJ 520, 859  
Langer N., 1991, A&A 243, 155  
Lee U., 2006, MNRAS 365, 677  
Lee U., Saio H., 1997, ApJ 491, 839  
Lighthill J., 1979, Waves in Fluids, Cambridge University Press, Cambridge  
MacGregor K.B., Charbonneau P., 1999, ApJ 519, 911  
McIntyre M.E., 2003, in "Perspectives in Fluid Dynamics: A Collective Introduction to Current Research", Eds. G.K. Batchelor, H.K. Moffat, M.G. Worster, Cambridge Univ. Press, 557  
Maeder A., 1995, A&A 299, 84  
Maeder A., 2003, A&A, 399, 263  
Maeder A., Meynet G., 2000, ARAA 38, 143  
Maeder A., Meynet G., 2004, A&A 422, 225  
Maeder A., Zahn J.-P. 1998, A&A 334, 1000  
Matias J., Zahn J.-P. 1998, Sounding solar and stellar interiors, IAU Symposium 181, Nice, Eds. J. Provost & F.X. Schmider  
Mathis S., 2005, PhD thesis, Université Paris VII  
Mathis S., Palacios A., Zahn J.-P., 2004, A&A 425, 243  
Mathis S., Zahn J.-P., 2005, A&A 440, 653  
Mestel L., 1953, MNRAS 113, 716  
Mestel L., Weiss N.O., 1987, MNRAS 226, 123  
Michaud G., 1993, Phys. Scripta T47, 143  
Michaud G., Charland Y., Vauclair S., Vauclair G., 1976, ApJ 210, 447  
Montalbán J., 1994, A&A 281, 421

- Montalbán J., Schatzman E., 1996, *A&A* 305, 513
- Montalbán J., Schatzman E., 2000, *A&A* 354, 943
- Nordlund A., Stein R.F., Brandenburg A., 1996, *Bull. Astron. Soc. of India* 24, 261
- Öpik E.J. 1951, *MNRAS* 111, 278
- Palacios A., Talon S., Charbonnel C., Forestini M., 2003, *A&A*, 399, 603
- Parker E.N., 1960, *ApJ* 132, 821
- Pinsonneault M.H., Kawaler S.D., Sofia S., Demarque P., 1989, *ApJ* 338, 424
- Pitts E., Tayler R.J., 1986, *MNRAS* 216, 139
- Press W.H., 1981, *ApJ* 245, 286
- Rayleigh Lord, 1880, *Proc. London Math. Soc.*, 11, 57
- Rayleigh Lord, 1916, *Proc. Roy. Soc. London* A93, 148
- Richard D. & Zahn J.-P., 1999, *A&A*, 347, 734
- Richer J., Michaud G., Rogers F., Iglesias C., Turcotte S., Leblanc F., 1998, *ApJ* 492, 833
- Richer J., Michaud G., Turcotte S., 2000, *ApJ* 529, 338
- Ringot O., 1998, *A&A* 335, 89
- Rogers T.M., Glatzmeier G.A., 2005a, *ApJ* 620, 432
- Rogers T.M., Glatzmeier G.A., 2005b, *MNRAS* 364, 1135
- Schatzman E., 1962, *An.Ap.* 25, 18
- Schatzman E., 1993, *A&A* 279, 431
- Schatzman E., Baglin A. 1991, *A&A* 249, 152
- Solberg H. 1936, *Procès-Verbaux Ass. Météor., UGGI, 6<sup>e</sup> Assemblée Générale, Edinburgh, Mém. et Disc.* 2, 66
- Spruit H.C., 1999, *A&A* 349, 189
- Spruit H.C., 2002, *A&A* 381, 923
- Stokes G.G., 1847, *Trans. Camb. Philos. Soc.* 8, 441
- Sutherland, B.R., Linden, F.R., 2002, *Phys. Fluids* 14, 721
- Sweet P.A. 1950, *MNRAS* 110, 548
- Talon S., 1997, “Hydrodynamique des étoiles en rotation”
- Talon S., Charbonnel C., 1998, *A&A* 335, 959
- Talon S., Charbonnel C., 2003, *A&A* 405, 1025
- Talon S., Charbonnel C., 2005, *A&A* 440, 981
- Talon S., Kumar P., Zahn J.-P., 2002, *ApJL* 574, 175
- Talon S., Richard O., Michaud D., 2006, *ApJ* 645, 634
- Talon S., Vincent A., Michaud G., Richer J. 2003, *J. Comp. Phys.* 184, 244
- Talon S., Zahn J.-P., 1997, *A&A* 317, 749
- Talon S., Zahn J.-P., Maeder A., Meynet G., 1997, *A&A* 322, 209
- Tassoul J.-L., Tassoul M., 1982, *ApJs* 49, 317
- Tassoul M., Tassoul J.-L., 1983, *ApJ* 271, 315
- Tayler R.J., 1973, *MNRAS* 161, 365
- Taylor G.I. 1923, *Phil. Trans. Roy. Soc.* A223, 289
- Toqué N., Lignières F., Vincent A., 2006, *GAFD* 100, 85

- Townsend A.A., 1965, *J. Fluid Mech.* 22, 241
- Townsend R.H.D., 2003, *MNRAS* 340, 1020
- Turcotte S., Richer J., Michaud G., Iglesias C.A., Rogers F.J., 1998, *ApJ* 504, 539
- Unno W., Osaki Y., Ando H., Saio H., Shibahashi H., 1989, "Nonradial oscillations of stars", 2<sup>nd</sup> edition, University of Tokyo Press
- Urpin V.A., Shalybkov D.A., Spruit H.C., 1996, *A&A* 306, 455
- VandenBerg D.A., Richard O., Michaud G., Richer J., 2002, *ApJ* 571, 487
- Vauclair S., 1983, *Astrophysical Processes in Upper Main Sequence Stars*, 13<sup>th</sup> SAAS-FEE course, Eds. B. Hauck & A. Maeder
- Vincent A., Michaud G., Meneguzzi M., 1996, *Phys. Fluids* 8 (5) 1312
- Vogt H., 1925, *Astron. Nachr.* 223, 229
- von Zeipel H., 1924, *MNRAS* 84, 665
- Weber E.J., Davis L., 1967, *ApJ* 148, 217
- Wendt F., 1933, *Ing. Arch.* 4, 577
- Young P.A., Knierman K.A., Rigby J.R., Arnett D., 2003, *ApJ* 595, 1114
- Zahn J.-P., 1975, *A&A* 41, 329
- Zahn J.-P. 1983, *Astrophysical Processes in Upper Main Sequence Stars*, 13<sup>th</sup> SAAS-FEE course, Eds. B. Hauck & A. Maeder
- Zahn J.-P., 1992, *A&A* 265, 115
- Zahn J.-P., Mathis S., Brun A.S., 2007, *A&A* submitted
- Zahn J.-P., Talon S., Matias J., 1997, *A&A* 322, 320